



Computationally Exploring and Alleviating the Kinetic Bottlenecks of Anaerobic Methane Oxidation

Matthew J. Grisewood¹, James G. Ferry² and Costas D. Maranas^{1*}

¹ Department of Chemical Engineering, Pennsylvania State University, University Park, PA, United States, ² Department of Biochemistry and Molecular Biology, Pennsylvania State University, University Park, PA, United States

OPEN ACCESS

Edited by:

Nidia S. Caetano,
Instituto Superior de Engenharia do
Porto (ISEP), Portugal

Reviewed by:

Naresh Singhal,
University of Auckland, New Zealand
Seung Gu Shin,
Pohang University of Science and
Technology, South Korea

*Correspondence:

Costas D. Maranas
costas@psu.edu

Specialty section:

This article was submitted to
Microbiotechnology, Ecotoxicology
and Bioremediation,
a section of the journal
Frontiers in Environmental Science

Received: 30 April 2018

Accepted: 05 July 2018

Published: 27 July 2018

Citation:

Grisewood MJ, Ferry JG and
Maranas CD (2018) Computationally
Exploring and Alleviating the Kinetic
Bottlenecks of Anaerobic Methane
Oxidation. *Front. Environ. Sci.* 6:84.
doi: 10.3389/fenvs.2018.00084

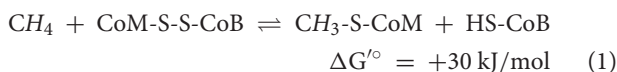
The anaerobic oxidation of methane (AOM) by methanotrophic archaea offers a carbon- and electron- efficient route for the production of acetate, which can be further processed to yield liquid fuels. This acetate production pathway is initiated by methyl-coenzyme M reductase, but this enzyme can only oxidize trace amounts of methane *ex situ*. Efforts to improve the kinetics of methyl-coenzyme M reductase through enzyme engineering have been, in part, limited by low-throughput assays. Computational enzyme engineering can circumvent this limitation through the design of smaller, more focused libraries, which have a higher probability of success. By drawing from a new consensus reaction mechanism for Mcr and newly published data, the first complete kinetic characterization of the Mcr reaction mechanism is proposed. In the developed kinetic description, the rate of methyl-coenzyme M unbinding is proposed to limit Mcr overall kinetics. A revised computational method was devised to improve the rate of product release while not disrupting the reaction's activated complex. Large, hydrophobic amino acids that can assume multiple conformations were predicted to be most effective at reaching this design goal. Other rate-limiting scenarios were examined, such as (i) high-temperature (>45°C), (ii) methyltransferase-limiting, and (iii) ineffective cofactor F₄₃₀ binding. A separate library of designs is put forth for each one of these cases. These efforts mark the first computational attempt at redesigning methyl-coenzyme M reductase for reversed or improved activity, which if experimentally validated, would have a cross-cutting impact across the biotechnology and biochemistry fields by debottlenecking anaerobic methane oxidation.

Keywords: methyl-coenzyme M reductase, Mcr, product release, anaerobic oxidation of methane, IPRO, enzyme, redesign

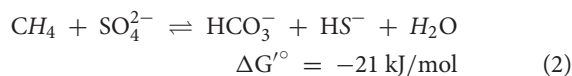
INTRODUCTION

Each year, marine sediments oxidize an estimated 70–300 teragrams of methane (Reeburgh, 1996; Hinrichs and Boetius, 2003) to form carbon dioxide (Knittel and Boetius, 2009), which is about 21 times less effective at trapping heat in the atmosphere (Ragsdale et al., 2017). Industrially mimicking this natural process enables the possibility of converting methane to liquid fuels in an efficient and environmentally friendly manner (Haynes and Gonzalez, 2014). Consortia of

ANAerobic METHanotrophic archaea (ANME) and sulfate-reducing bacteria are responsible for the anaerobic oxidation of methane (AOM) in these sediments (Knittel and Boetius, 2009; Shima et al., 2012). The key enzyme for methane activation is a homolog of methyl-coenzyme M reductase (Mcr)—an enzyme that catalyzes anaerobic methanogenesis—that runs in reverse (Hoehler et al., 1994; Krüger et al., 2003; Hallam et al., 2004; Moran et al., 2005; Scheller et al., 2010; Shima et al., 2012). ANME Mcr couples the endergonic oxidation of methane to methyl-coenzyme M (CH₃-S-CoM) with the reduction of coenzyme M-coenzyme B heterodisulfide (CoM-S-S-CoB, HDS) to coenzyme B (HS-CoB, see Equation 1; Harmer et al., 2008; Thauer, 2011).



The ANME in marine sediments directly donate electrons to their syntrophic sulfate-reducing bacteria partner via nanowire-like structures (McGlynn et al., 2015; Wegener et al., 2015; Scheller et al., 2016). This electron transfer yields a thermodynamically favorable net reaction (Equation 2; Thauer, 2011), but this free energy change is unlikely to support growth of both organisms (Thauer and Shima, 2008).



Alternative electron acceptors [such as iron (III), manganese (IV), chromium (VI), and nitrate] are more energetically favorable than sulfate (Beal et al., 2009; Haroon et al., 2013; Mueller et al., 2015; Lu et al., 2016; Nazem-Bokaei et al., 2016; Soo et al., 2016) and can ensure thermodynamic feasibility of AOM.

Methanogenic Mcrs are ($\alpha\beta\gamma$)₂ hexamers that include two highly conserved active sites, where the nickel-containing cyclic tetrapyrrole prosthetic group known as cofactor F₄₃₀ is non-covalently bound (Ermler et al., 1997; Grabarse et al., 2000). For methanogenesis, CH₃-S-CoM must bind prior to HS-CoB to form a ternary complex (Wongnate and Ragsdale, 2015), and the nickel of cofactor F₄₃₀ must be present in the Ni(I) state (Goubeaud et al., 1997). The ordered binding for Mcr is facilitated through numerous important enzyme conformational changes (Grabarse et al., 2001; Cedervall et al., 2010; Ebner et al., 2010). Mcr methanogenesis is initiated through homolytic cleavage of CH₃-S-CoM to yield methyl radical and Ni(II)-thiolate intermediates (Chen et al., 2012; Scheller et al., 2013; Wongnate et al., 2016). This radical mechanism is also feasible for AOM, consistent with the “reverse methanogenesis” hypothesis (Krüger et al., 2003; Hallam et al., 2004; Moran et al., 2005, 2007; Nauhaus et al., 2005; Heller et al., 2008; Knittel and Boetius, 2009; Scheller et al., 2010; Chen et al., 2012; Wongnate et al., 2016). Though trace AOM in methanogens has been demonstrated (Moran et al., 2005, 2007; Scheller et al., 2010), the reported specific AOM rate of a methanogenic Mcr was 7-fold lower than that of ANME Mcr (Scheller et al., 2010). This is consistent with Mcr limiting overall AOM

kinetics. By improving the activity of Mcr, the economics for the carbon- and energy-efficient bioconversion of methane to liquid fuels becomes more propitious (Haynes and Gonzalez, 2014).

Improving enzyme activity is typically attained through directed evolution approaches that mandate high-throughput screening of large variant libraries (Bloom et al., 2005; Packer and Liu, 2015). High-throughput screening is streamlined through the use of a simple assay, such as a chromogenic or fluorogenic substrate or sensor (see Xiao et al., 2015 for review). Such a simple assay for AOM by Mcr does not currently exist. AOM Mcr activity has only been monitored using limited throughput techniques that include isotopic labeling (Moran et al., 2005, 2007; Scheller et al., 2010; Soo et al., 2016) and cell growth on methane (Soo et al., 2016). The complexity of the Mcr system—exemplified by its many post-translational and cofactor modifications (Ermler et al., 1997; Grabarse et al., 2000; Shima et al., 2012; Allen et al., 2014), cofactor synthesis (Zheng et al., 2016), and oxidative inactivation (Goubeaud et al., 1997)—makes it extremely challenging to study *in vitro* and thus further limits the gamut of available assays. These limitations motivate the use of rational approaches to design small, focused libraries with a higher likelihood of success. Various rational approaches, such as site saturation mutagenesis or manual rational design, are also inapt for Mcr because of its complex chemistry and the inability to focus on one or two variable positions.

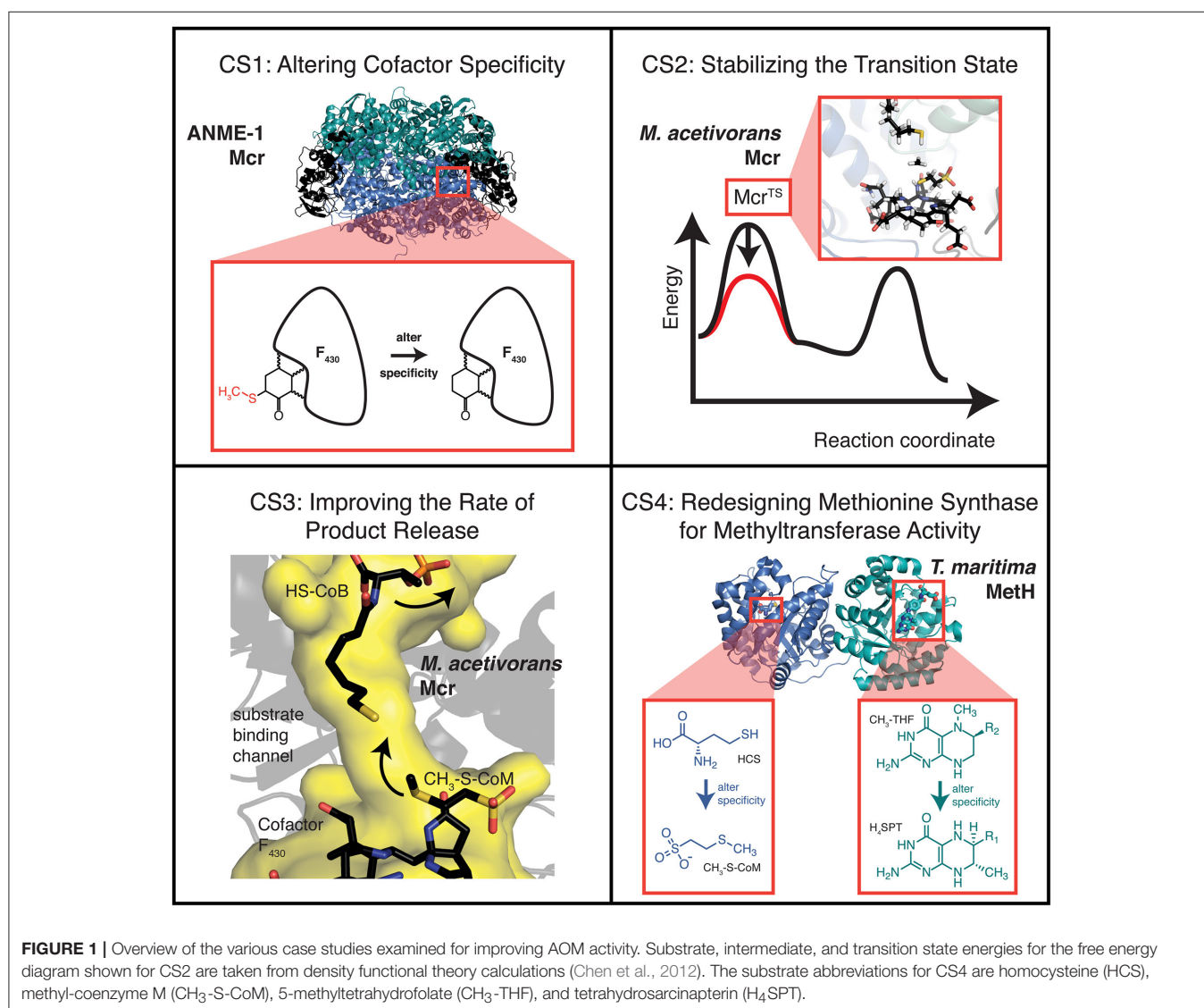
A robust approach to rationally engineer Mcr for improved catalytic activity is computational enzyme redesign. Several types of computational procedures have been successfully deployed for enzyme engineering, including *de novo* (Jiang et al., 2008; Röthlisberger et al., 2008; Faiella et al., 2009; Siegel et al., 2010; Richter et al., 2012; Garrabou et al., 2016), structure-based (Ashworth et al., 2006; Murphy et al., 2009; Grisewood et al., 2017), and sequence-based approaches (Moore and Maranas, 2004; Meyer et al., 2006; Pantazes et al., 2007) (see refs. Pantazes et al., 2011; Hilvert, 2013; Huang et al., 2016 for review). Structure-based redesign is best suited for the aim of improving AOM activity because Mcr, which has a known structure (Shima et al., 2012), naturally catalyzes this reaction (Moran et al., 2005, 2007; Scheller et al., 2010). The Iterative Protein Redesign and Optimization procedure (IPRO) is a structure-based protein redesign tool that incorporates (step 1) recursive random backbone perturbations, (step 2) deterministic rotational isomer (i.e., rotamer) optimizations, and structural refinements to improve enzyme performance toward a specific target (Saraf et al., 2006; Fazelinia et al., 2007; Grisewood et al., 2013; Pantazes et al., 2015). These structural refinements include (step 3) local ligand docking and (step 4) a force field energy minimization. Designs then have (step 5) their interaction energies with various ligands calculated, and based on these calculated energies, (step 6) the variant is accepted or rejected using the Metropolis criteria. IPRO offers key advantages over other available structure-based redesign procedures in that it can (i) handle multiple design criteria simultaneously, (ii) be easily manipulated for a problem-specific objective function, and (iii) maintain the geometry of catalytic residues using distance restraints.

In this work, we investigated the limiting steps for AOM kinetics and developed multiple case studies under which different steps may be limiting. For each of these case studies, *Methanosarcina acetivorans* serves as the host system because ANME methanotrophs have not yet been isolated (Scheller et al., 2010; Haynes and Gonzalez, 2014). *M. acetivorans* is phylogenetically closely related to ANME-2 (a specific clade of ANME; Mueller et al., 2015) archaea (Moran et al., 2007; Yan et al., 2018). The goal of improving AOM kinetics was subdivided into four separate case studies. The first case study (CS1) considered redesigning ANME-1 Mcr to accept the cofactor F₄₃₀ found in methanogenic archaea in lieu of its native cofactor (Mayr et al., 2008; Shima et al., 2012). In a second case study (CS2), we considered that Mcr may be limited by formation of the methyl radical at high temperatures (>45°C; Wongnate et al., 2016). In the third study (CS3), published Mcr binding and reaction rates were used to postulate that Mcr kinetics is limited by CH₃-S-CoM unbinding (Ellermann et al., 1988; Scheller et al., 2010; Chen et al., 2012; Wongnate and Ragsdale, 2015; Wongnate

et al., 2016). A final investigation (CS4) examined the possibility that AOM is limited by the second step of the reverse aceticlastic pathway involving a methyl-tetrahydrosarcinapterin:coenzyme M (CH₃-H₄SPT:HS-CoM) methyltransferase (Mtr) (Benedict et al., 2012; Vepachedu and Ferry, 2012; Nazem-Bokaei et al., 2016). An overview of these case studies is provided in **Figure 1**.

RESULTS AND DISCUSSION

For each case study, we constructed enzyme variant libraries to alleviate its particular kinetic limitation. Execution of various case studies is important for improving AOM kinetics because the precise relationship between physical conditions and the rate-limiting step is ill-defined. We describe general trends observed in the variant libraries for each case study and analyze differences between the libraries. The top results for each library are presented in each case.



Case Study 1: Altering Anme-1 Mcr Cofactor Specificity

The recently elucidated structure of ANME-1 Mcr (Shima et al., 2012) revealed key structural differences relative to methanogenic Mcrs. These differences included enriched regions of cysteine residues, a methylthiolation of cofactor F₄₃₀ at C17², and a distinct set of post-translationally modified amino acids (Shima et al., 2012). While the significance of each of these differences has not been fully resolved, it is reasonable to assume that they arose from evolutionary divergence or fine-tuning of the enzyme for its specific function. It has been suggested that the 17²-methylthiolation of cofactor F₄₃₀ is catalytically non-essential because ANME-2 Mcrs contain the unmodified cofactor (Mayr et al., 2008). Moreover, the importance of Mcr's post-translational modifications has been questioned since many of these adaptations are not conserved (Kahnt et al., 2007). In CS1, the assumption is made that these post-translational and cofactor modifications help to maintain the proper active site geometry but are non-essential for catalytic activity.

Expression of ANME-1 Mcr into the *M. acetivorans* host and subsequent AOM was recently demonstrated (Soo et al., 2016). Although ANME-1 Mcr in *M. acetivorans* was not isolated and activity validated, wild-type (WT) *M. acetivorans* is unable to perform AOM in the absence of methanogenic substrates indicating methane consumption of the engineered strain is attributable to ANME-1 Mcr and not WT Mcr (Soo et al., 2016). However, the methane consumption by ANME-1 Mcr corresponds to an AOM specific activity of only ~20 nmol min⁻¹ mg⁻¹ (Soo et al., 2016), which is about 3-fold lower than the estimated *in vivo* activity of ANME Mcr (Scheller et al., 2010). The assumption that the 17²-methylthiolation of cofactor F₄₃₀ is crucial for locking the cofactor into its preferred orientation in ANME-1 Mcr implies a reduction in catalytic activity ensues if cofactor F₄₃₀ is not correctly oriented. Therefore, the reduced activity of ANME-1 Mcr expressed in *M. acetivorans* may be partially explained by the unavailability of the methylthiolated cofactor in methanogens (Mayr et al., 2008; Allen et al., 2014). Improving ANME-1 Mcr binding to the unmodified cofactor could engender increased rates for AOM when the enzyme is expressed in *M. acetivorans*.

IPro was used to predict ANME-1 Mcr variants with improved binding to the unmodified cofactor F₄₃₀. Variable positions (i.e., design positions) were selected based on (i) proximity to C17², (ii) conservation amongst methanogens but not methanotrophs, and (iii) a review of existing literature, which suggested V419 is crucial for the C17² methylthiolation (Shima et al., 2012) (see Materials and Methods). The 10 selected design positions were Q72, L77, M78, N90, P149, I154, H157, H414, V419, and C423, which all reside within the α -subunit of ANME-1 Mcr. Five independent IPro trajectories were simulated for 1000 iterations using ensemble structure refinements. Ensemble structure refinements are used within IPro to sample multiple confirmations for a given protein sequence, thereby improving the accuracy of the energy calculations and quality of the results. During the five IPro simulations, eight unique variants were identified. The top five variants are provided in Table 1.

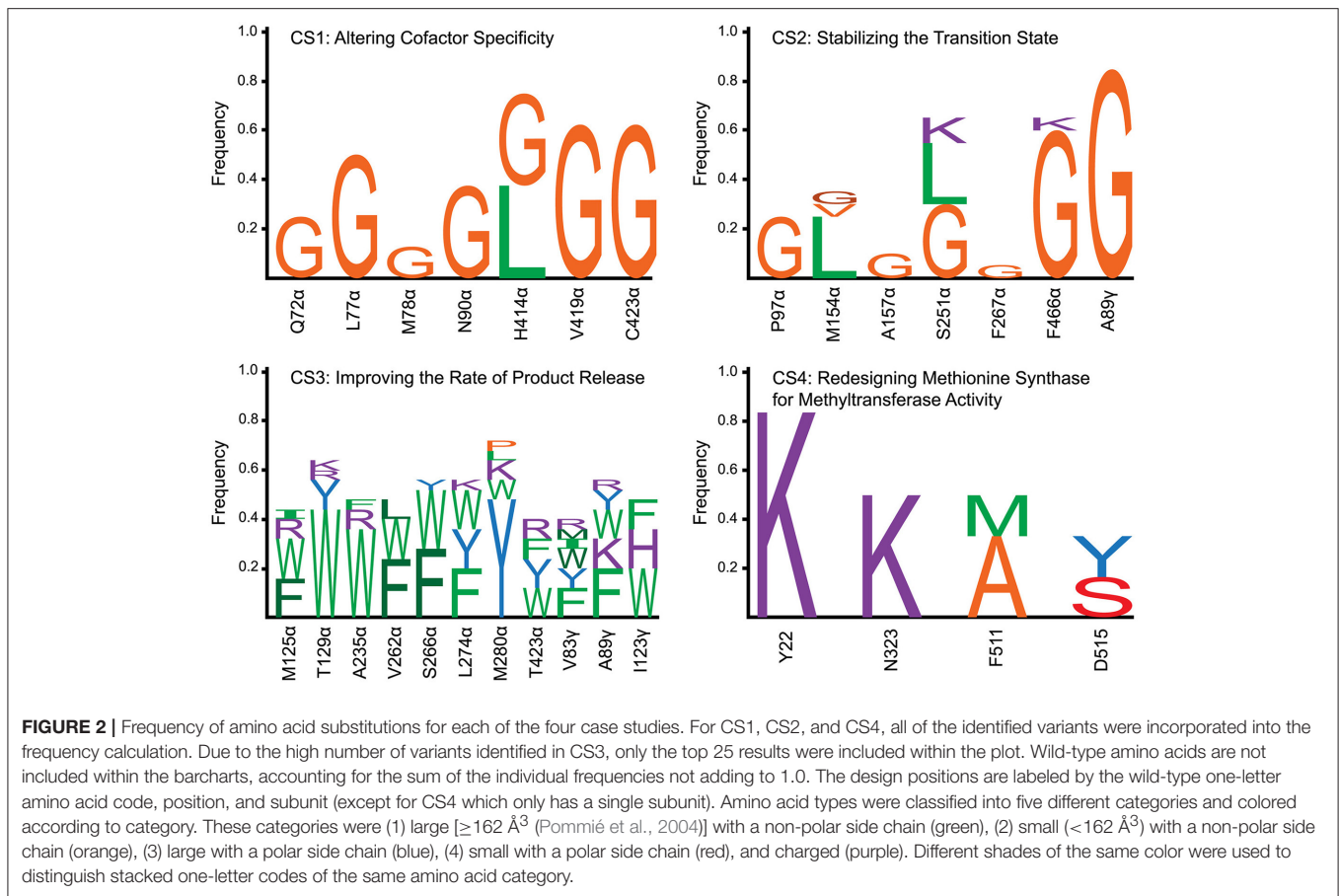
In examining the top five variants presented in Table 1, a propensity for glycine substitutions was observed (see Figure 2). At first, it was thought that these substitutions were algorithmic artifacts due to unfavorable backbone conformations or to alleviate steric clashes within the active site. Despite introducing a Lennard-Jones softening term and reweighting the scoring function for the rotamer optimization step (i.e., step 2 of IPro; Grisewood et al., 2017), this partiality for glycine persisted. Additionally, the same algorithmic architecture was employed for CS2–CS4 and for a separate enzyme system (Grisewood et al., 2017), but this glycine preference was not observed in those studies. Based on this and analyzing the top structures, it seems plausible that the glycine residues provide the required flexibility within the active site that allows other side chains to form beneficial contacts with the unmodified cofactor F₄₃₀.

The geometry of the top variants' active sites appears at an intermediate state between ANME-1 Mcr and *Methanothermobacter thermautotrophicus* (i.e., methanogenic) Mcr with their native cofactors (see Figure 3). It is unsurprising that the top ANME-1 variants do not bind cofactor F₄₃₀ as tightly as *M. thermautotrophicus* because the methanogenic Mcr has naturally evolved to tightly bind its cofactor. Additionally, V419 is replaced with a methylated (presumably to increase the active site hydrophobicity) glutamine in the *M. thermautotrophicus* structure. IPro is limited in that it can only replace the valine with canonical amino acids, and in this case, hydrophobic amino acids. This restricts the gamut of possible side chain conformations within the tightly packed and highly conserved Mcr active site. Despite not achieving the same level of tight binding to cofactor F₄₃₀ relative to *M. thermautotrophicus*, the top variants demonstrate a noticeable improvement over ANME-1 Mcr in terms of the calculated interaction energies. The two closest design positions to C17² are H414 and V419, which constitute the methylthio- substituent's binding site in ANME-1 Mcr. Unlike *M. thermautotrophicus* Mcr that occupies the methylthio- binding site via a large side chain at position 419, IPro suggests redesigns that shift the side chain of position 414 closer to C17² (see Figure 3). Variants that do not contain the H414G substitution (i.e., Variants 3 and 5, see Table 1), instead

TABLE 1 | Top five variants of CS1, sorted by interaction energy between the enzyme and unmodified cofactor F₄₃₀.

Variant	1*	2*	3*	4*	5
Q72	–	G	–	–	–
L77	–	G	G	G	–
M78	–	–	–	G	–
N90	G	–	–	G	–
H414	G	G	L	–	L
V419	–	–	G	G	–
C423	G	–	G	G	–

No substitutions were observed for design positions P149, I154, and H157. All design positions were within the α -subunit of ANME-1 Mcr and are sorted by the interaction energy between the variant and cofactor F₄₃₀. An asterisk next to the variant number indicates a significant improvement over WT interaction energy ($p < 0.05$).



force V419 closer to C17², although not to the extent of the methyl-glutamine in *M. thermautotrophicus*. The effect of the other substitutions is more subtle since these design positions are more distant from the active site.

The veracity of these results is dependent on two key assumptions. First, the ANME-1 Mcr post-translational modifications must be non-essential because the genes required to make these modifications may not exist within the host organism. Second, the 17²-methylthiolation of cofactor F₄₃₀ ought to be catalytically insignificant. Since these two assumptions cannot be tested *a priori*, we considered a second case study that focused on identifying the kinetic bottleneck and redesigning the native Mcr of *M. acetivorans*, where the concerns of heterologous expression are eliminated.

Developing a Complete Model for Mcr Kinetics

The complex chemistry undergone during Mcr catalysis has attracted numerous investigations into the enzyme's reaction mechanism, and recent findings have shown that Mcr follows a bi-bi radical-based reaction mechanism (Cedervall et al., 2010; Chen et al., 2012; Scheller et al., 2013; Wongnate and Ragsdale, 2015; Wongnate et al., 2016). This information, along with several assumptions, an existing IC₅₀ value for HDS during

methanogenesis (Ellermann et al., 1988), and the rate of ¹³CH₃-S-CoM formation as a function of methane partial pressure (Scheller et al., 2010), yielded specific rate constants for each step in the mechanism. One key assumption in the development of this model is that Mcr kinetics is nearly invariant amongst various methanogenic archaea. This assumption, which is supported by very strong sequence conservation (Reeve et al., 1997) and nearly identical active site structures (Grabarse et al., 2000), enables integration of extensive data to fully characterize Mcr kinetics. These observed and estimated rate constants suggest the probable rate-limiting step of Mcr, which is the release of the produced CH₃-S-CoM to regenerate the free enzyme.

The full reaction mechanism of Mcr, including substrate binding and product release, is depicted in **Figure 4**. The specific rate constant for step 1 was estimated using inhibition studies (Ellermann et al., 1988) and is discussed in greater detail below. Density functional theory calculations (Chen et al., 2012) and the Eyring equation were used to estimate the specific rate constants for step 2. While the transition state for step 3 was not found, the anionic intermediate (Mcr^{Int1}) was only "transiently formed" and thus its kinetics must be rapid (Chen et al., 2012). The kinetics of step 4 is evaluated from fitting data to the Michaelis-Menten equation and is described in more detail below (Scheller et al., 2010). The specific rate constant for step 5 was also calculated from density functional theory calculations and the

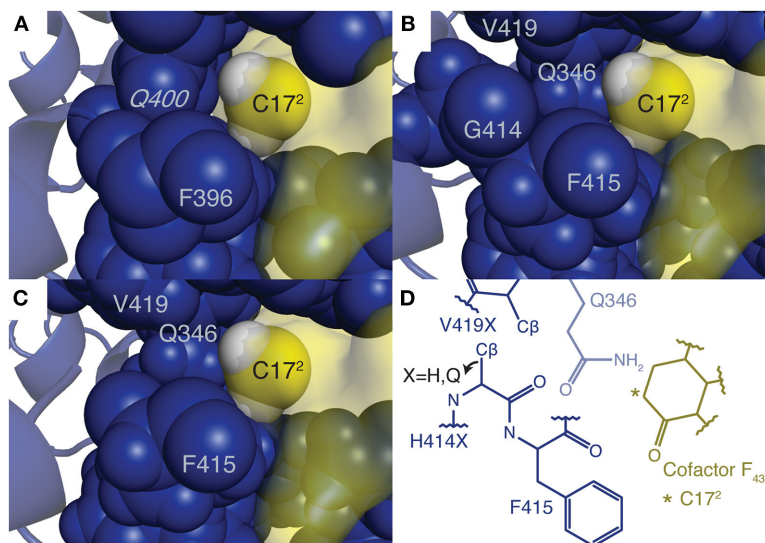


FIGURE 3 | Active site structures of (A) *M. thermautotrophicus* Mcr, (B) the top CS1 variant, (C) ANME-1 Mcr, and (D) an overview of all three Mcrs in complex with cofactor F₄₃₀. In subplots (A–C), the unmodified cofactor F₄₃₀ is depicted as a yellow molecular surface with C17² and its two bonded hydrogen atoms (colored white) shown as spheres. Residues within six angstroms of C17² are displayed as blue spheres, while the remainder of the enzyme is represented by a blue cartoon diagram. G416 and G417 (G397 and G398 in *M. thermautotrophicus* Mcr) are not shown so that the spatial relationship between C17² and nearby amino acids is clearly visible. Residues constituting the methylthio- substituent binding site in the ANME-1 structure are labeled by their one letter amino acid abbreviation and sequence position, including the methylated glutamine (italicized). The C17² carbon is also labeled. Due to the highly conserved structures of the three Mcrs, subplot D was created, which depicts the general architecture of the active site. Residues forming the methylthio- moiety binding site are labeled using the numbering scheme of ANME-1 Mcr (Q346, H414, F415, and V419 correspond to Q332, Q395, F396, and methyl-Q400 in *M. thermautotrophicus*, respectively). Q346 is behind the other the amino acids, which is represented by its reduced opacity. The position of the C β is given for the second hydrogen atom in H414G (as in the top variant of CS1), but the C β position shifts away from C17² if a larger side chain is present.

Eyring equation (Chen et al., 2012). Step 6 does not have an energy barrier and therefore also exhibits a fast reaction rate (Chen et al., 2012). The specific rate constants for steps 7 and 8 of the mechanism are taken from electron paramagnetic resonance (EPR) and fluorescence experiments (Wongnate and Ragsdale, 2015). Calculations for steps 2 and 5 assumed a temperature of 25°C to match the EPR and fluorescence conditions (Wongnate and Ragsdale, 2015).

The kinetics of step 1 was estimated using competitive inhibition studies by HDS during methanogenesis, where an IC₅₀ of 0.6 mM was reported (Ellermann et al., 1988). The mechanism for HDS inhibition is depicted in Figure 5. k_{12} in Figure 5 is equivalent to k_1 (the rate constant for step 1 of methanotrophy) in Figure 4. Assuming Briggs-Haldane kinetics (i.e., reaction intermediate concentrations are time invariant) and that the concentration of Mcr-HDS formed via reaction 11 is negligible relative to that of reaction 12, k_{12} can be expressed as a function of the IC₅₀ value (Equations 3, 4, see Supplementary Material).

$$k_{12} = \frac{k_{-12} + \frac{k_{-12}(k_{-10} + k_{11})}{k_{10}[\text{HS-CoB}]} + C_1 k_{-12} \left(1 + \frac{k_{13}[\text{HS-CoB}]}{k_{-13}}\right)}{\text{IC}_{50} C_1} \quad (3)$$

$$C_1 = \frac{k_{11}}{k_9 [\text{CH}_3\text{-S-CoM}]} + \frac{k_{-9}(k_{-10} + k_{11})}{k_9 k_{10} [\text{CH}_3\text{-S-CoM}] [\text{HS-CoB}]} \quad (4)$$

The underlying assumption that Mcr-HDS is primarily formed through reaction 12 (see Figure 4) is justified because methane formation (i.e., the reaction co-product) is considerably reduced in the presence of HDS (Ellermann et al., 1988), and this assumption also implies that $k_{-12} > 18 \text{ s}^{-1}$ (k_{cat} for methanogenesis) (Wongnate and Ragsdale, 2015). The known HDS IC₅₀ value (Ellermann et al., 1988), the corresponding substrate concentrations (Ellermann et al., 1988), and known specific rate constants (Wongnate and Ragsdale, 2015) establish a lower limit for k_{12} ($1.08 \times 10^6 \text{ M}^{-1} \text{ s}^{-1}$). Using the IC₅₀ value (0.6 mM) as an approximate HDS concentration, we can estimate the specific rate constant for step 1 as 650 s^{-1} .

The specific rate constant for step 4 was determined using the hyperbolic dependence of reaction velocity on methane concentration ($R^2 = 0.998$), which is indicative of Michaelis-Menten kinetics (Scheller et al., 2010). Methane partial pressures (Scheller et al., 2010) were converted to concentrations using the linear relationship between concentration and pressure under moderate conditions (1–20 bar, $R^2 = 1.000$, see Supplementary Figure 1; Duan and Mao, 2006). The *in vivo* Mcr concentration (4.7 μM) was estimated from carbon monoxide-activated *Methanothermobacter marburgensis* cells (Zhou et al., 2013). Non-linear regression was used to estimate Michaelis-Menten parameters for the reaction ($k_{\text{cat}} = 0.12 \text{ s}^{-1}$, $K_M = 2.5 \text{ mM}$, see Supplementary Figure 2). Established from the same experimental studies as steps 7 and 8, the lower limit for the k_{off} rate is 20 s^{-1} (Wongnate and Ragsdale, 2015). Using the

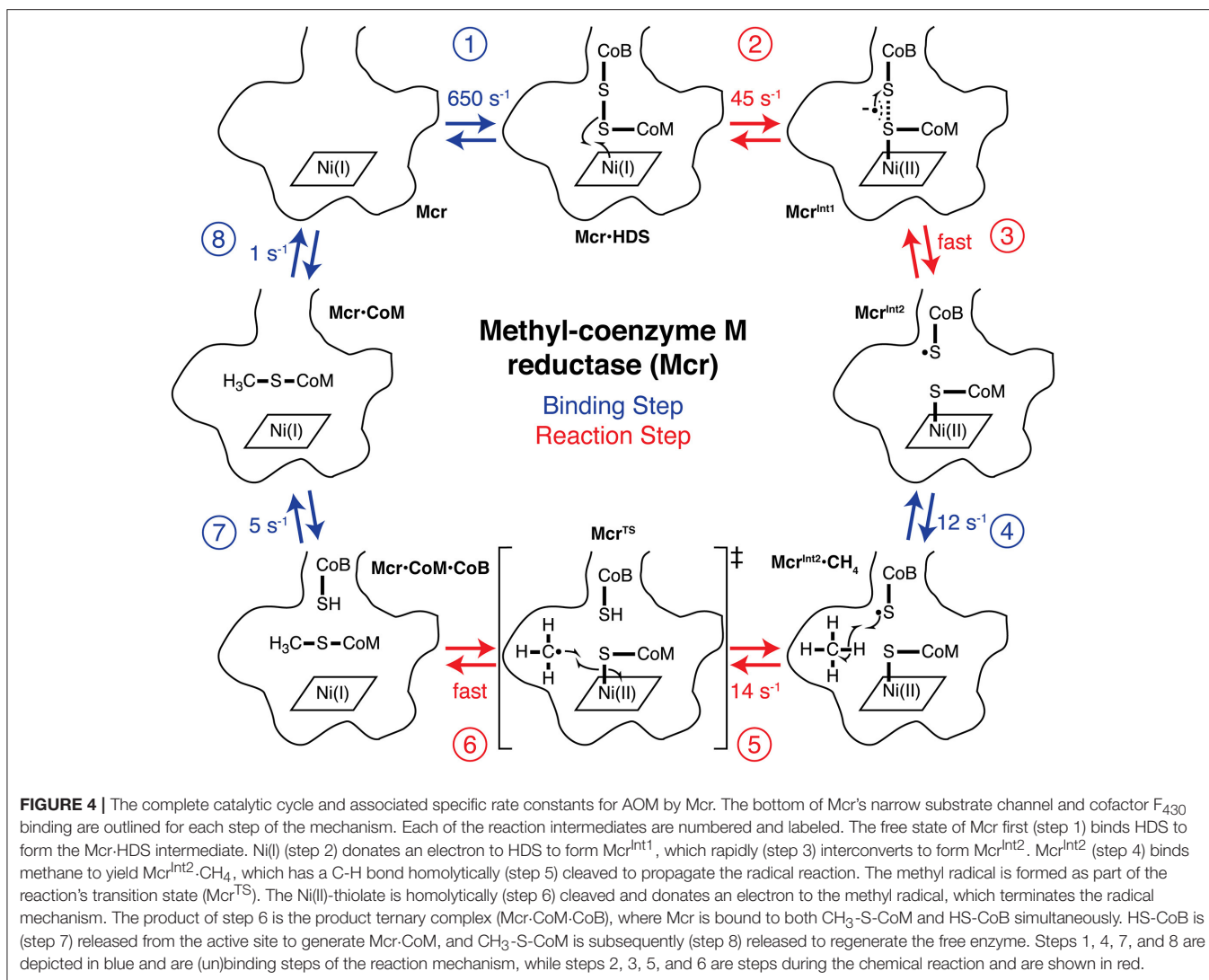


FIGURE 4 | The complete catalytic cycle and associated specific rate constants for AOM by Mcr. The bottom of Mcr's narrow substrate channel and cofactor F₄₃₀ binding are outlined for each step of the mechanism. Each of the reaction intermediates are numbered and labeled. The free state of Mcr first (step 1) binds HDS to form the Mcr-HDS intermediate. Ni(I) (step 2) donates an electron to HDS to form Mcr^{Int1}, which rapidly (step 3) interconverts to form Mcr^{Int2}. Mcr^{Int2} (step 4) binds methane to yield Mcr^{Int2}·CH₄, which has a C-H bond homolytically (step 5) cleaved to propagate the radical reaction. The methyl radical is formed as part of the reaction's transition state (Mcr^{TS}). The Ni(II)-thiolate is homolytically (step 6) cleaved and donates an electron to the methyl radical, which terminates the radical mechanism. The product of step 6 is the product ternary complex (Mcr·CoM·CoB), where Mcr is bound to both CH₃-S-CoM and HS-CoB simultaneously. HS-CoB is (step 7) released from the active site to generate Mcr·CoM, and CH₃-S-CoM is subsequently (step 8) released to regenerate the free enzyme. Steps 1, 4, 7, and 8 are depicted in blue and are (un)binding steps of the reaction mechanism, while steps 2, 3, 5, and 6 are steps during the chemical reaction and are shown in red.

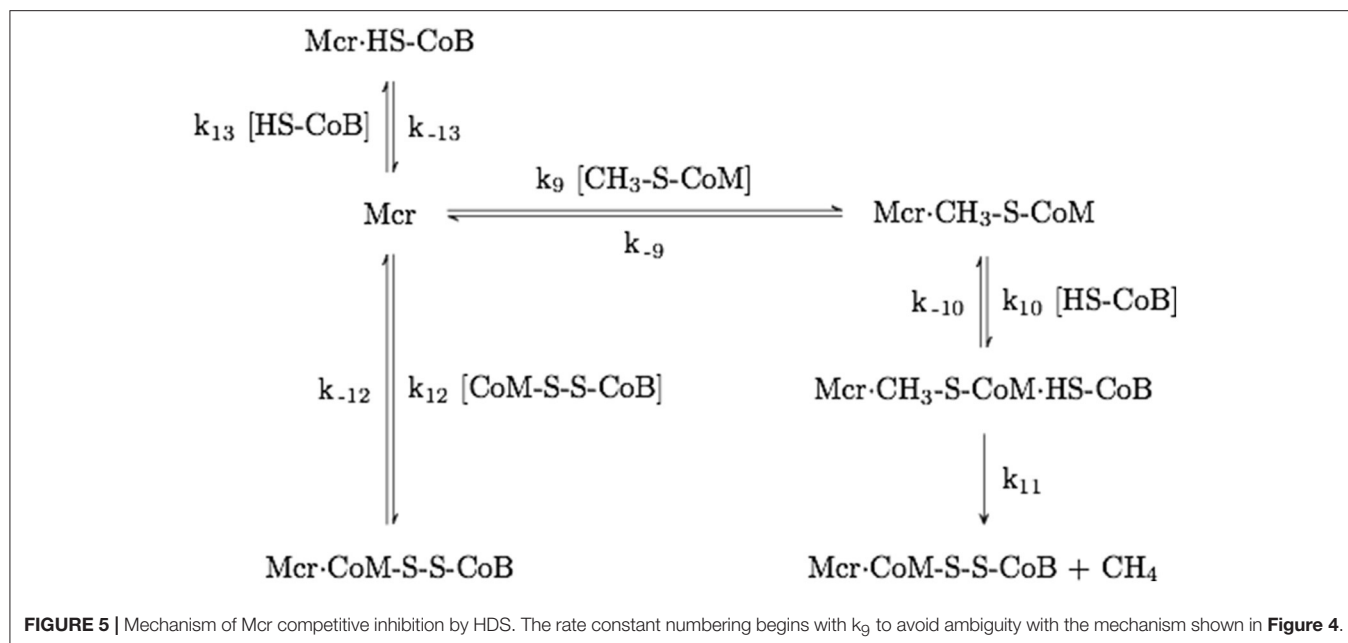
established k_{off} , k_{cat} , and K_{M} values, the k_{on} rate constant can be calculated ($k_{\text{on}} = 7.9 \text{ mM}^{-1} \text{ s}^{-1}$). At 25°C and atmospheric pressure, the methane concentration is $\sim 1.5 \text{ mM}$ (Duan and Mao, 2006). Therefore, the lower limit of the specific rate constant for step 4 is found to be 12 s^{-1} .

Case Study 2: Stabilizing the Transition State of *M. acetivorans* Mcr

While the developed model suggests product release limits Mcr AOM kinetics, it is conceivable that under a different set of physical conditions, a separate step of the mechanism could constrain the net reaction rate. This theory gains credence due to the biphasic kinetics of methyl radical formation in Mcr, which is thought to be a result of a structural transition at 30°C (Wongnate et al., 2016). Above 30°C, the entropy of activation is $\sim -56 \text{ J mol}^{-1} \text{ K}^{-1}$ (Wongnate et al., 2016). This indicates that the energy barrier for step 5 increases (slower reaction rate) with increasing temperature beyond 30°C. Alternatively, product dissociation from enzymes (i.e., steps 7 and 8 for Mcr) are

expected to have a near-zero entropy of activation (Kamerlin et al., 2008), indicating that the energy barrier is insensitive to temperature changes. Since the specific rate constant for step 5 of the reaction mechanism is only marginally larger than that of the reported rate of product release (step 8), it seems plausible that the formation of the methyl radical would constrain the net rate for AOM at higher temperatures ($>45^\circ\text{C}$). In Case Study 2, Mcr variants are identified that stabilize the transition state (Mcr^{TS}), which corresponds to formation of the methyl radical.

Methanosarcina acetivorans Mcr variants were selected by IPRO with the objective function targeting an improvement in interaction energy with the transition state. Design positions were chosen on the basis of (i) proximity to the active site, and (ii) sequence diversity amongst methanogens (see Materials and Methods). The nine selected design positions were P97 α , M154 α , A157 α , M163 α , I245 α , S251 α , F267 α , F466 α , and A89 γ . The transition state structure (Chen et al., 2012) was grafted into the *M. acetivorans* Mcr active site, with atoms from the resolved transition state structure fixed in place. Grafting the



transition state structure resulted in an unfavorable Generalized Born implicit solvation energy term (Lee et al., 2003) for the enzyme that was not readily alleviated with a force field energy minimization. Interaction energies were used in lieu of complex energies to ensure that stabilization of the transition state does not also stabilize the ground state molecules, and render the energy barrier unaltered. Ten independent IPRO trajectories were simulated for 3000 iterations each, and 20 total variants were established. The top five variants are enumerated in **Table 2**.

Table 2 demonstrates that substitution with leucine at position M154 α and a substitution with glycine at A89 γ are ubiquitous. The WT Mcr structure reveals an unfavorable hydrophilic-hydrophobic contact between R152 γ and A89 γ (4.8 Å between the guanidino group of R152 γ and C β of A89 γ). The substitution to glycine alleviates this poor contact due to its lower hydrophobicity and longer distance to R152 γ (5.2 Å). The A89 γ G substitution does not interact with the transition state. The other ubiquitous substitution, M154 α L, indirectly removes a poor interaction with the transition state structure of cofactor F₄₃₀ (unmodified in CS2–CS4). The leucine side chain forces Q244 α into an alternate conformation with respect to the WT structure. In the WT structure, two amido groups are in close proximity (one from cofactor F₄₃₀, one from Q244 α), weakening nearby hydrogen bonds between Mcr and cofactor F₄₃₀. When Q244 α is in its alternate conformation, caused by M154 α L, these hydrogen bonds remain intact, improving the interaction energy between Mcr and the grafted transition state.

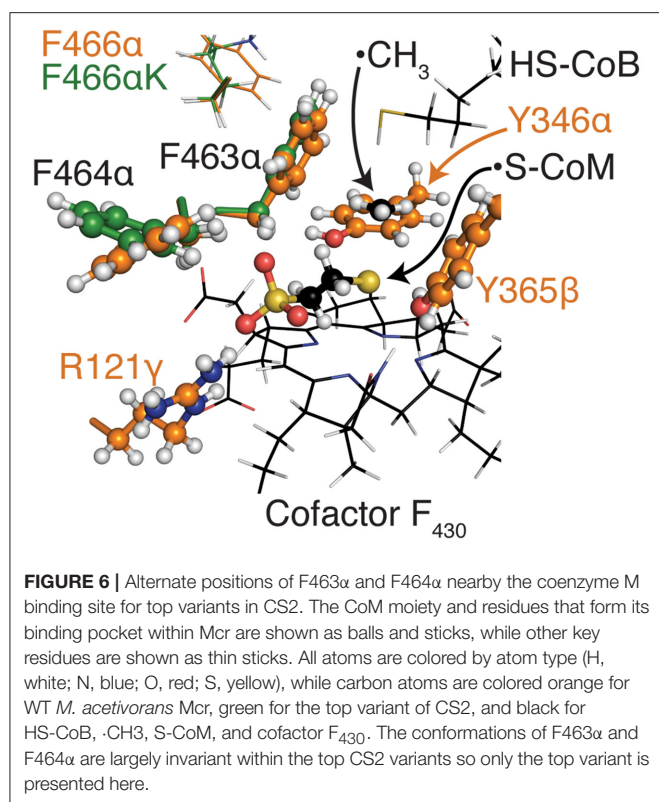
The top designs listed in **Table 2** suggest that the presence of S251 α K, S251 α L, and S251 α G can all form beneficial interactions with the transition state. Though the nature of these side chains vary drastically, they all improve interaction energy by stabilizing a nearby loop of residues between M255 α and G258 α , which is immediately adjacent to cofactor F₄₃₀. S251 α K stabilizes this loop by forming a hydrogen bond between the

TABLE 2 | Top five variants of CS2, sorted by interaction energy between the enzyme and grafted transition state.

Variant	1*	2*	3*	4*	5*
M154 α	–	L	L	–	L
S251 α	K	K	L	L	G
F466 α	K	G	G	G	–
A89 γ	G	G	G	G	G

Design positions are listed with their WT one-letter amino acid code, followed by sequence position and Mcr subunit. No substitutions were observed at P97 α , A157 α , M163 α , I245 α , and F267 α . Variants were sorted by their interaction energy with the transition state. An asterisk is provided next to variants with significant improvements over WT ($p < 0.05$).

S251 α K ϵ -amino hydrogen and the unprotonated nitrogen of H145 α . S251 α L stabilizes the M255 α -G258 α loop by packing nicely within a binding site formed by M72, H73, T149, V159, and A252, all of which constitute the α -subunit. Finally, S251 α G forms favorable dispersion forces with V159 α , which is sandwiched between the loop and S251 α . Design position F466 α can accommodate substitutions to lysine or glycine in order to improve interaction energy with the grafted transition state. Similar to the S251 α substitutions, both F466 α K and F466 α G stabilize the transition state by altering the conformation of residues lining the long, narrow substrate channel of Mcr. The residues with the most drastic changes are F463 α , F464 α , Q469 α , N501 α , and H504 α , where F463 α and F464 α form part of the \cdot S-CoM binding site. Since phenylalanine is hydrophobic and \cdot S-CoM is largely hydrophilic, the altered conformation reduces unfavorable hydrophobic-hydrophilic interactions in the active site, thereby improving the interaction energy with the transition state. In this alternate conformation, more hydrophilic amino acids, such as Y346 α , Y365 β , and R121 γ , can create favorable contacts with \cdot S-CoM in its binding pocket (see **Figure 6**).



In all, the top five CS2 designs converge to the same principles to improve interaction energy with the transition state. Substitutions at M154 α (only leucine) help improve the hydrogen bonding network between Mcr and cofactor F₄₃₀. The substitutions at S251 α stabilize the conformation of the loop between M255 α and G258 α , which directly contacts cofactor F₄₃₀. F466 α K and F466 α G reduce the hydrophobicity nearby the hydrophilic \cdot S-CoM. The substitution at position A89 γ does not affect transition state binding but instead lessens an unfavorable contact formed with R152 γ .

Case Study 3: Engineering *M. acetivorans* Mcr for More Rapid Product Release

Case Study 3 was carried out to improve the rate of CH₃-S-CoM and HS-CoB unbinding, which are proposed to be the first and second slowest steps, respectively, of the reaction mechanism at 25°C. Though a transition state structure is unattainable for (un)binding events, the energy barrier can be lowered by raising the energy of the ground state Mcr-CoM-CoB and Mcr-CoM complexes. Destabilization of the enzyme's ground state has been demonstrated to improve catalysis for other enzyme systems (Andrews et al., 2013; Ruben et al., 2013; Phillips et al., 2016) and is particularly applicable for improving the rate of product release, where finding a transition state structure is impractical. Mcr-CoM-CoB and Mcr-CoM exhibit similar enzyme topologies and CH₃-S-CoM binding modes, with the key difference being increased flexibility in the Mcr substrate channel nearby the HS-CoB binding site (Cedervall et al., 2010). The low backbone

root-mean-square deviation (RMSD) between Mcr-CoM-CoB and Mcr-CoM of 0.21 Å, with a ligand all-atom RMSD of 0.07 Å, supports this claim (Grabarse et al., 2001; Cedervall et al., 2010). Owing to this high structure similarity, variants that destabilize Mcr-CoM are expected to correspondingly destabilize Mcr-CoM-CoB. By destabilizing Mcr-CoM-CoB, the rates of both CH₃-S-CoM and HS-CoB unbinding (i.e., steps 7 and 8) are expected to increase.

The structures of Mcr^{TS} and Mcr-CoM-CoB are also similar, with a ligand all-atom RMSD of 1.7 Å. Due to this similarity, it was postulated that increasing the complex energy of Mcr-CoM-CoB might also destabilize Mcr^{TS}. The variant structures from CS2 were used to test this hypothesis, and a strong correlation was observed between the two energies ($r = 0.73$). To account for this, IPRO's objective function was adjusted so as to minimize the difference in Mcr^{TS} and Mcr-CoM-CoB complex energies. Additionally, an alternate conformation of the β -subunit between residues 364 and 370 persists in the free enzyme (Grabarse et al., 2001) near the HS-CoB binding site. A constraint was added to IPRO to prevent destabilization of the free enzyme (Mcr), while incorporating the structural differences in the β -subunit between Mcr and Mcr^{TS}/Mcr-CoM-CoB.

A description of the revised MILP used within the second step of an IPRO iteration is provided below:

Sets

$i, j \in \{1, 2, \dots, N\}$ = Set of perturbed positions in Mcr α - and/or γ - subunits

$r, s \in \{1, 2, \dots, R_i\}$ = Set of rotamers, where R_i is the number of rotamers available at position i

$k, l \in \{1, 2\}$ = Binding assemblies

A binding assembly is a set of ligands that has its binding affinity for the design molecule (i.e., Mcr) altered by IPRO. Each structure within the Mcr mechanism (see **Figure 4**) signifies a separate binding assembly. For CS3, there are three binding assemblies: (1) Mcr^{TS}, (2) Mcr-CoM-CoB, and (3) the unbound enzyme (i.e., Mcr). Only the first two binding assemblies are considered in the revised MILP. The third binding assembly is used within a subsequent MILP with its rotamers restricted to match the amino acid sequence from the first MILP's optimal solution (see Pantazes et al., 2015 for a more detailed description of the standard IPRO MILP). Thus, two MILPs are executed within a single IPRO iteration.

Binary Variables

$$x_{irk} = \begin{cases} 1, & \text{if rotamer } r \text{ is selected at position } i \text{ in binding assembly } k \\ 0, & \text{otherwise} \end{cases}$$

Continuous Variables

$$z_{irkjs} = \begin{cases} 1, & \text{if rotamer } r \text{ is selected at position } i \text{ and rotamer } s \\ & \text{is simultaneously selected at position } j \text{ in binding assembly } k \\ 0, & \text{otherwise} \end{cases}$$

Parameters

E_{irk}^{rc} = rotamer – constant energy of rotamer r at position i in binding assembly k

E_{irkjs}^{rr} = rotamer – rotamer energy between rotamer r at position i and rotamer s at position j in binding assembly k

Am_{irk} = amino acid type of rotamer r at position i in binding assembly k

The rotamer-constant energy is the energy between a rotamer and any other non-rotamer atom within a single binding assembly (e.g., ligands and protein backbone). Using these defined sets, binary variables, continuous variables, and parameters, the MILP objective function is shown in Equation (5), subject to the constraints provided as Equations (6)–(9).

$$\text{Minimize } \sum_{i=1}^N \sum_{r=1}^{R_i} (x_{ir1} E_{ir1}^{rc} - x_{ir2} E_{ir2}^{rc}) - \sum_{i=1}^{N-1} \sum_{j>i}^N \sum_{r=1}^{R_i} \sum_{s=1}^{R_j} (z_{ir1js} E_{ir1js}^{rr} - z_{ir2js} E_{ir2js}^{rr}) \quad (5)$$

$$Am_{irk} = Am_{irl}, \forall i, r, k < l \quad (6)$$

$$\sum_{r=1}^{R_i} x_{irk} = 1, \forall i, k \quad (7)$$

$$x_{irk} = \sum_{s=1}^{R_j} z_{irkjs}, \forall i, r, k, j > i \quad (8)$$

$$x_{jks} = \sum_{r=1}^{R_i} z_{irkjs}, \forall i, s, k, j > i \quad (9)$$

The objective function (Equation 5) minimizes the difference in complex energy between MCr^{TS} and MCr·CoM·CoB. Equation (6) guarantees that the same amino acid type is used at each position in both binding assemblies. Equation (7) ensures that only one rotamer is selected at each position. The continuous variable, z_{irkjs} , can be written as the product of the two binary variables ($x_{irk} \times x_{jks}$) and is linearized by Equations (8) and (9).

Since the designs from CS2 did not directly interact with the substrate, we reconsidered the design positions for CS3. The design positions for CS3 were selected based on (i) proximity to the active site or the β -subunit between residues 364 and 370, where the conformation varies between MCr and MCr^{TS}/Mcrc·CoM·CoB, (ii) amino acid diversity at the position, and (iii) proper orientation of the side chain toward either the multi-conformational β -subunit loop or the active site (see Materials and Methods). The 10 selected design positions for CS3 were M125 α , T129 α , A235 α , V262 α , S266 α , L274 α , M280 α , T423 α , V83 γ , and A89 γ . As was the case for CS2, transition state atoms for the first binding assembly were fixed in place. The third binding assembly that ensures $E(\text{Mcrc}_{\text{variant}}) \leq E(\text{Mcrc}_{\text{WT}})$ permitted the use of complex energies instead of interaction

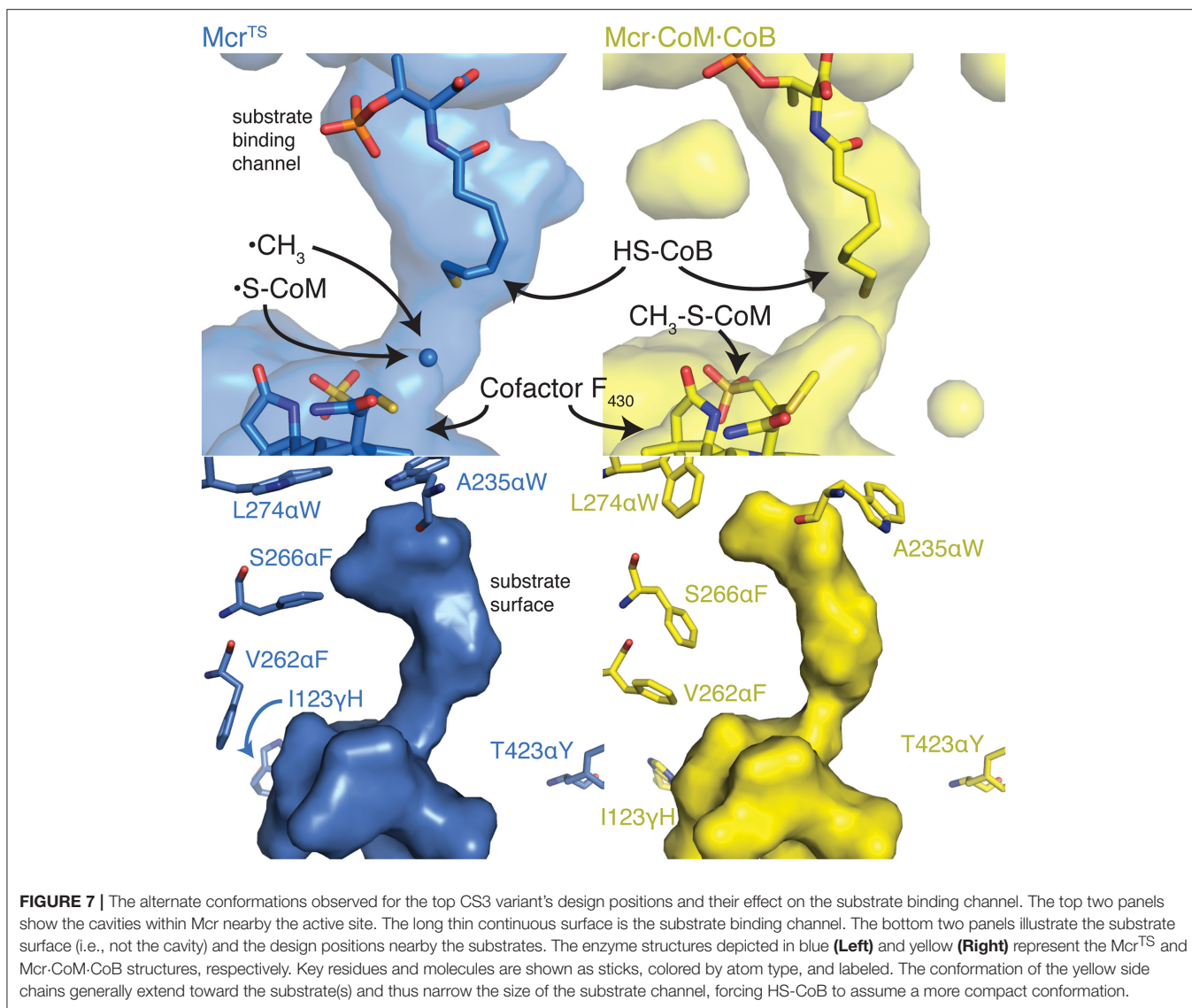
energies (that were used for CS2). Ten independent IPRO trajectories were executed for 100 iterations each, and 45 variants were identified. The decision to use a fewer number of iterations was made retroactively due to the large success rate and time-consuming nature of ensemble refinements (each refinement performed costs 250 additional IPRO iterations). Of the 45 identified variants, 15 showed simultaneous improvement in stabilizing MCr^{TS} and destabilizing MCr·CoM·CoB. The top five of these 15 variants, which were sorting by ascending [$E(\text{Mcrc}_{\text{TS}}) - E(\text{Mcrc} \cdot \text{CoM} \cdot \text{CoB})$] values, are presented as **Table 3**.

Table 3 shows a preference for large hydrophobic amino acids (see **Figure 2**). The hydrophobic tendency is unsurprising because of the hydrophobic nature of the MCr active site, but the large size of the substituted amino acids was unexpected due to the small accessible volume available within the active site. In analyzing the top structures presented in **Table 3**, these variants notably demonstrate alternate conformations when the rotamer in the MCr^{TS} binding assembly versus the MCr·CoM·CoB binding assembly. In general, when the variant is in the MCr^{TS} state, the side chain does not extend toward the narrow substrate binding channel. However, when the variant is in the MCr·CoM·CoB state, the side chain does extend toward the narrow substrate channel, partially occluding it. From a mechanistic point of view (see **Figure 4**), it is plausible that the conformational change of these residues helps to initiate product unbinding by “pushing” the products out of the active site via steric clashes. These side chains likely demonstrate a high degree of flexibility, evidenced by their different conformations in the two binding assemblies, and their overall non-specific interactions formed in both binding assemblies (see **Figure 7**). It is expected that the high flexibility of these residues drives product unbinding but similarly will likely slow the substrate binding of HDS (methane is likely small enough to still pass through the channel). Fortunately, since the predicted specific rate constant is two orders of magnitude higher for substrate binding (see **Figure 4**), these effects will likely go unnoticed since substrate binding still be unlikely to limit

TABLE 3 | Top five variants for simultaneously improving the rate of product release and stabilizing the transition state.

Variant	1*	2*	3*	4*	5*
M125 α	–	–	W	–	–
T129 α	K	Y	W	–	–
A235 α	W	W	–	W	–
V262 α	F	F	–	F	W
S266 α	F	F	–	F	F
L274 α	W	F	–	F	F
M280 α	Y	Y	–	Y	Y
T423 α	Y	W	–	W	–
V83 γ	F	F	–	–	–
A89 γ	–	–	W	–	–
I123 γ	H	H	–	H	–

Design positions are listed within their one-letter amino acid abbreviation, position, and MCr subunit. All variants are sorted by [$E(\text{Mcrc}_{\text{TS}}) - E(\text{Mcrc} \cdot \text{CoM} \cdot \text{CoB})$] values. An asterisk next to the variant number signifies a significant improvement relative to WT ($p < 0.05$).



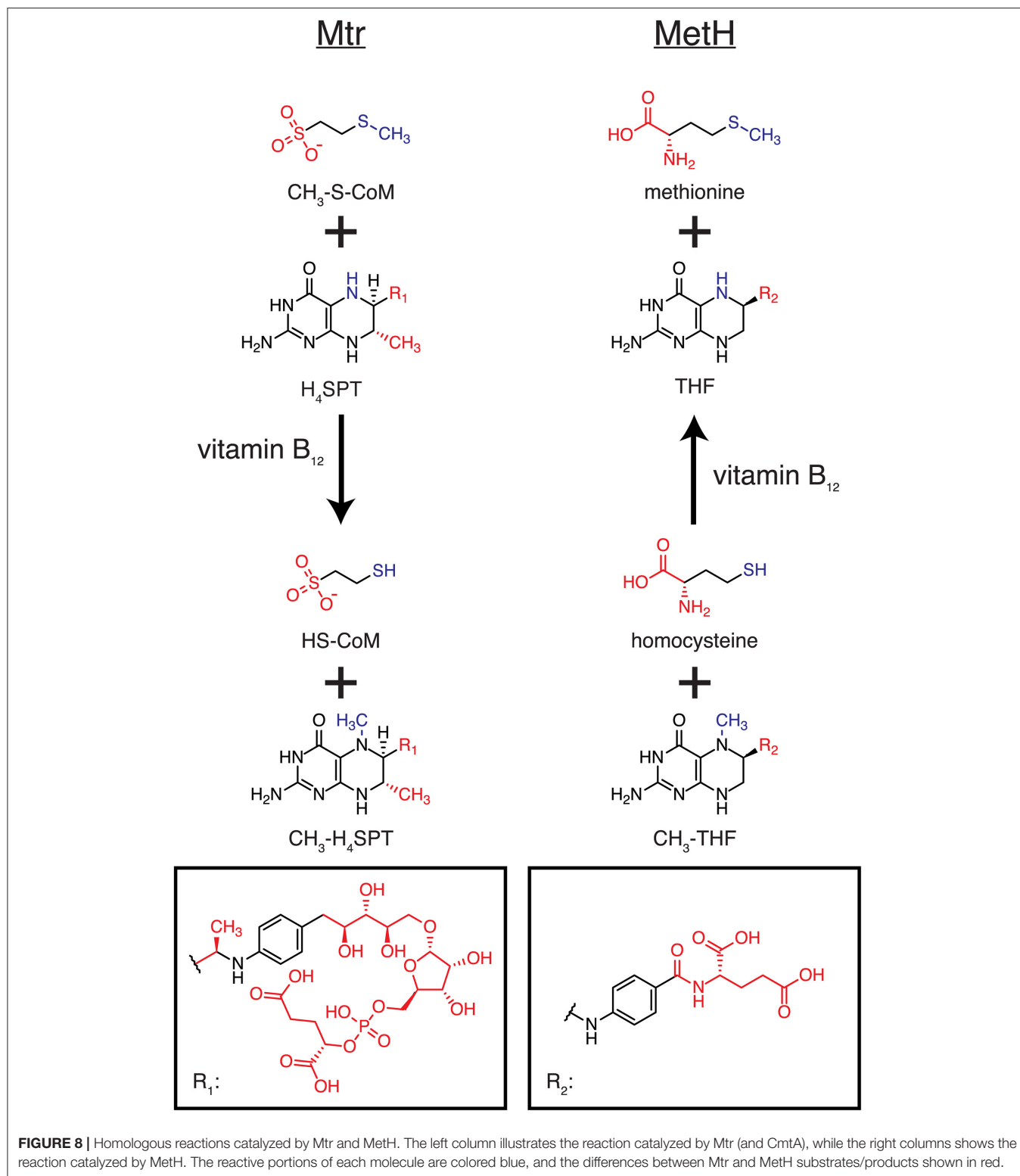
the overall AOM. Another key difference between Mcr^{TS} and Mcr-CoM-CoB is the more compact aliphatic chain conformation of HS-CoB in the Mcr-CoM-CoB state of the enzyme. Finally, it is noted that the WT structures, even after refinement, do not demonstrate multiple conformations in a similar manner as the variant structures.

Case Study 4: Converting *E. coli* Methionine Synthase Into a Mtr

One final possibility that was considered is that Mcr does not limit the overall AOM kinetics, but instead, the second step of the reverse acetoclastic pathway catalyzed by Mtr may constrain the net reaction rate. Mtr, a transmembrane protein, catalyzes the transfer of a methyl group from CH₃-H₄SPT to HS-CoM and presumably catalyzes the reverse reaction for AOM. Although a soluble version of Mtr (CmtA) was discovered (Vepachedu and Ferry, 2012), this enzyme does not have a known structure and has not demonstrated reversibility, which is essential for

inclusion in the AOM pathway. Moreover, homology modeling is unlikely to produce a reliable structure due to low sequence identity of available templates, where the best template covers < 60% of the CmtA sequence space and exhibits only 16% sequence overlap with CmtA (Arnold et al., 2006). Due to these problems associated with CmtA, an alternative approach is to redesign an enzyme homolog with an established structure.

One of the closest homologs to CmtA is methionine synthase (MetH), which catalyzes the transfer of a methyl group from 5-methyltetrahydrofolate to homocysteine to form tetrahydrofolate and methionine (Altschul et al., 1997). Both CmtA and MetH employ vitamin B₁₂ as a cofactor for the reaction. CmtA catalyzes the transfer from an aliphatic methyl thioether to a pteridine ring, yielding a thiol, and methylated pteridine ring. Similarly, MetH transfers a methyl moiety from a methylated pteridine ring to a thiol, producing a methyl thioether and pteridine ring (see **Figure 8**). Additionally, MetH has a resolved crystal structure of its N-terminal domain, where 5-methyltetrahydrofolate and



homocysteine bind (PDB 1Q8J) (Evans et al., 2004), and these binding sites are distant from the enzyme's catalytic machinery (Evans et al., 2004). The specific activity of MetH is about 2-fold higher than that of CmtA (Huang et al., 2007; Vepachedu and

Ferry, 2012) and is approximately equal between the forward and reverse directions (Rüdiger and Jaenicke, 1969). The similarity of the chemical reaction to that of Mtr, its known crystal structure, cytosolic localization, and high specific activity make

TABLE 4 | Top five variants predicted to alter MetH specificity in efforts to mimic the reaction catalyzed by Mtr.

Variant	1*	2*	3*	4*	5*
Y22	K	K	K	K	K
N323	–	–	K	K	–
F511	M	–	A	–	A
D515	–	–	Y	S	–

No substitutions were observed for design positions K72, D105, E320, E345, N360, N538, D541, and E542. Design position Y22 is in the CH₃-S-CoM binding domain, while the remaining design positions constitute part of the H₄SPT binding domain. All variants were sorted by their interaction energies with the Mtr substrates. An asterisk next to the variant number denotes a significant improvement in interaction energy over WT ($p < 0.05$).

MetH a very attractive target for protein engineering. Case Study 4 aims at redesigning the MetH 5-methyltetrahydrofolate and homocysteine binding pockets to instead accommodate H₄SPT and CH₃-S-CoM, respectively.

MetH variants that demonstrate improved binding to H₄SPT and CH₃-S-CoM were found by running IPRO for 1,500 iterations over 10 independent trajectories using ensemble structure refinements. Design positions were selected on the basis of (i) distance to atoms that differ between CH₃-S-CoM and homocysteine or H₄SPT and 5-methyltetrahydrofolate, (ii) sequence diversity as determined using family sequence alignments, and (iii) unfavorable contacts formed between the WT residue at this position and the novel substrates (see Materials and Methods). Twelve design positions were selected in total. A slightly larger number of design positions were permitted due to the large distance between the binding sites. Y22, K72 and D105 were selected from the CH₃-S-CoM binding domain, while E320, N323, E345, N360, F511, D515, N538, D541, and E542 were selected from the H₄SPT binding domain. Prior to performing a production run, the WT structure was refined with the new substrates to remove as many bad contacts as possible before redesigning the enzyme. In the subsequent production run, six variants were identified with improved binding to the new substrates. The top five designs are presented in **Table 4**.

Table 4 reveals only one substitution made within the CH₃-S-CoM binding domain of MetH – Y22K (see **Figure 2**). As shown in **Figure 9**, this substitution is introduced to help stabilize the negative charge of the CH₃-S-CoM sulfonate group. In addition to the improved electrostatics, this conformation allows for hydrogen bonds to be formed between the protein backbone and the sulfonate. These hydrogen bonds are absent from the WT structure. The positive charge of Y22K is important because there are no other positively charged residues nearby to stabilize the sulfonate.

In the H₄SPT-binding domain, N323K forms a salt bridge with D390. This interaction stabilizes the wall of the binding crevice and also provides additional volume in the binding site to accommodate one of the methyl substituents that exist in H₄SPT but not THF. Both F511M and F511A open up a cavity in the binding site, similar to the N323K substitution. In addition, both F511M and F511A push N508 toward the carbonyl group of the H₄SPT pteridine substituent. This movement allows a more

favorable hydrogen bond to be formed between the carbonyl and N508. Both D515Y and D515S contribute to improving the stability of the binding site by creating a network of T-shaped π - π stacking interactions, including Y518 and Y519.

MATERIALS AND METHODS

Modeling of Enzyme and Ligand Structures

Two of the initial enzyme structures were adopted from crystallography experiments. The initial structure of ANME-1 Mcr (CS1) was taken from PDB 3SQG (Shima et al., 2012). Post-translational modifications were removed from the structure, as there is no way to ensure the presence of these modifications when heterologously expressed. The initial structure of MetH (CS4) was adopted from the N-terminal domain (residues 1–566) of *Thermotoga maritime* expressed in *Escherichia coli* [PDB 1Q8J] (Evans et al., 2004)]. The WT structure of *M. acetivorans* Mcr (CS2, CS3) was generated using homology modeling (Arnold et al., 2006), with *M. barkeri* Mcr as the template structure (each subunit $\geq 90\%$ sequence identity; Grabarse et al., 2000). For the alternate conformation of the β -subunit between residues 364 and 370, the amino acid sequences of the red-1 silent form (free Mcr) of *M. thermautotrophicus* Mcr and *M. acetivorans* Mcr are identical. The two flanking positions on each side of the loop were superimposed to the existing *M. acetivorans* structure, creating the model for the unbound form of Mcr used within CS3.

For CS1, the position of cofactor F₄₃₀ was determined by superimposing against the crystallized methylthiolated cofactor within ANME-1 Mcr. For CS2, the Mcr side chains that were included in transition state structure (Chen et al., 2012) were used to graft the transition state into the *M. acetivorans* Mcr structure by minimizing the RMSD between the transition state and homology modeled structure. The positions of the remaining atoms that were not included in the model of the transition state (i.e., atoms distant from the reactive portions of the molecules) were modeled using CHARMM's internal coordinate system. For CS3, the CH₃-S-CoM, HS-CoB, and cofactor F₄₃₀ coordinates were modeled by superimposing against the ox-1 silent version of *M. thermautotrophicus* Mcr (Grabarse et al., 2001). For CS4, the homologous portions between CH₃-S-CoM and homocysteine, as well as between H₄SPT and 5-methyltetrahydrofolate were superimposed. Docking tools were then used to further refine the initial placement of the structures.

Design Position Selection

One of the main criteria used for design position selection for all of the case studies was a family sequence alignment. All sequence alignments were performed using Clustal-Omega (Sievers et al., 2011). The sequences to be aligned were extracted from the conserved domain database for CS2–CS4 (Marchler-Bauer et al., 2015). For CS1, differences between methanogenic and methanotrophic archaea were used and therefore manually curated (since methanogenic Mcr and methanotrophic Mcrs are still homologous). The methanogenic Mcr sequences were taken from Uniprot codes P07962, P22948, A4PJ22, D3E050, P12971, P11558, O27232, Q49605, Q58256, P11559, P07961, and

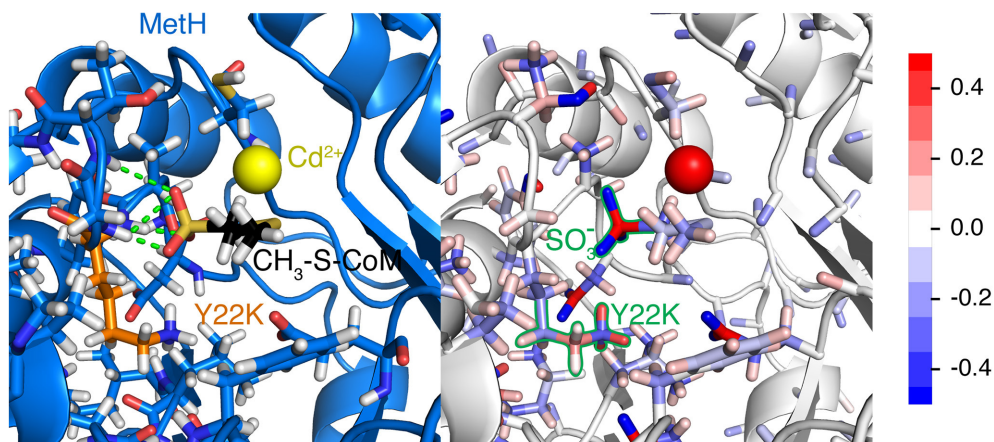


FIGURE 9 | Y22K substitution observed in each of the top five variants for CS4. The **(Left)** panel depicts the hydrogen bonds (green) formed between the Mcr backbone and the sulfonate group. Mcr is shown as a blue cartoon, with active site residues colored by element and represented by sticks. Y22K and CH₃-S-CoM are also shown as sticks with their carbon atoms colored orange and black, respectively. The cadmium ion in the active site is shown as a yellow sphere. The **(Right)** panel shows the same representation of the active site, but atoms are instead colored by partial charge. It is evident that there is a strong negative charge of the sulfonate group and a positive charge of the Y22K (keeping in mind that the positive charge is distributed amongst the H atoms). The scale for the color scheme is shown on the far right of the figure.

Q6LWZ5 (UniProt, 2015). The methanotrophic Mcr sequences were codes Q6VUA6, Q64E03, Q64EA1, Q648C5, Q64D16, D1JBK4, Q6MZD1, Q64CB7, Q64AN3, Q64EF1, Q649Z5, and Q64DN6. Only those positions that were observed in $\geq 75\%$ of the methanotrophs and $< 45\%$ of the methanogens were considered for CS1. For CS2–CS4, design positions were considered sufficiently diverse if their sequence conservation was $\leq 70\%$.

Distances calculated to the active site were measured from the nickel atom of cofactor F₄₃₀, or the sulfur atoms of CH₃-S-CoM or HS-CoB, whichever was closest. For CS3, the C β atoms of the altered loop in the β - subunit were also considered in the distance calculation, and for CS2, the atoms from the transition state model were used exclusively. For CS3, the dot product was taken at each position between the C α –C β vector and the vector between the C α carbon and closest atom from the aforementioned distance screen. Positions whose dot product was < 0.5 indicated that this residue was oriented away from the active site, and these positions were not permitted to serve as design positions for CS3. In CS4, unfavorable interactions associated with introducing a larger substrate into the MethH binding site were considered. The rotamer-constant energy was calculated at each position and only those with an unfavorable interaction (i.e., a positive value) remained a potential design position for CS4.

Case Study Details

The CHARMM force field parameters were determined using the parameter files of homologs and with the aid of CGenFF (Vanommeslaeghe and MacKerell, 2012; Vanommeslaeghe et al., 2012). The Lazaridis-Karplus solvation files were created using the parameters during the model's construction (Lazaridis and Karplus, 1999). Each of the case studies incorporated multiple IPRO trajectories, an ensemble of variants to reliably estimate

CHARMM energies, and on the order of $\sim 1,000$ iterations. Fewer iterations were used for CS3 due to the high percentage of successful variants. The ensemble of structures provided distributions of energy values, which were statistically analyzed using Welch's *t*-test. Two copies of the α - subunit, one copy of the β - subunit, and one copy of the γ -subunit form an active site for Mcr. For CS1, only the α - subunits were considered because the β - and γ - subunits are not nearby the C17² atom. For CS2, all four polypeptides were incorporated as design molecules (i.e., molecules that can have their structures perturbed). For CS3, the multiple β - subunit conformations were used to take advantage of subtle active site differences between the free and bound enzymes. Therefore, the β - subunit was considered a target molecule (along with HS-CoB, CH₃-S-CoM, and cofactor F₄₃₀), while the two α - subunits and γ -subunit were still considered design molecules. MethH only consists of one chain and was modeled as such. CS1–CS3 incorporated IPRO's dimer constraint, which ensures that the design positions are equally perturbed and varied for each polypeptide chain. The remaining IPRO parameters were set to their default values. All IPRO parameters for each case study are provided in **Table 5**.

CONCLUSIONS

The AOM by archaea is a complex reaction cascade that is still not fully elucidated (Thauer, 2011; Nazem-Bokae et al., 2016). Though a consensus mechanism for AOM has been agreed upon, the role of conformational changes, post-translational modifications, the role of symbiotic partnerships, and the kinetics for the full reaction remain unknown. Adding to this complexity is the inherently challenging reaction catalyzed by Mcr, which breaks a stable C-H bond without the use of oxygen-derived

TABLE 5 | IPRO input parameters for CS1–CS4.

Parameter	CS1	CS2	CS3	CS4
Design molecules	A. ANME-1 Mcr, α 1 D. ANME-1 Mcr, α 2	A. MA Mcr, α 1 B. MA Mcr, β C. MA Mcr, γ D. MA Mcr, α 2	A. MA Mcr, α 1 C. MA Mcr, γ D. MA Mcr, α 2	H. <i>E. coli</i> Meth
Target molecules	GS B. HS-CoB F. cofactor F ₄₃₀ M. CH ₃ -S-CoM	TS F. cofactor F ₄₃₀ M. CH ₃ -S-CoM O. HS-CoB	B. Bound MA Mcr, β U. Unbound MA Mcr, β TS F. cofactor F ₄₃₀ M. CH ₃ -S-CoM O. HS-CoB PS P. cofactor F ₄₃₀ Q. CH ₃ -S-CoM R. HS-CoB	GS C. active site Cd ²⁺ M. CH ₃ -S-CoM P. H ₄ SPT T. active site H ₂ O
Binding assemblies	1. Improve binding to F 2. Maintain binding to B and M	1. Improve binding to F, M, and O	1. Improve complex energy with B, F, M, and O 2. Worsen complex energy with B, P, Q, and R 3. Maintain binding to F and U	1. Improve binding to C, M, P, and T
Design positions	A and D. Q72, L77, M78, N90, P149, I154, H157, H414, V419, and C423	A and D. P97, M154, A157, M163, I245, S251, F267, and F466 C. A89	A and D. M125, T129, A235, V262, S266, L274, M280, and T423 C. V83 and A89	H. Y22, K72, D105, E320, N323, E345, N360, F511, D515, N538, D541, and E542
Refinement used?	Yes	No	Yes	Yes
Independent trajectories	5	10	10	10
Iterations per trajectory	1,000	3,000	100	1,500
Force field	CHARMM	CHARMM	CHARMM	CHARMM
Topology file	mcr_top.rtf	mcr_top.rtf	mcr_top.rtf	meth_top.rtf
Parameter file	mcr_par.prm	mcr_par.prm	mcr_par.prm	meth_par.prm
Solvation file	mcr_sol.dat	mcr_sol.dat	mcr_sol.dat	meth_sol.dat
Extra constraints	1. Dimer constraint between A and D 2. All atoms in B, F, and M fixed in place	1. Dimer constraint between A and D 2. Fixed atoms in A (Q161), B (Y365), D (Y346), F (all), M (all), and O (all)	1. Dimer constraint between A and D 2. Fixed atoms in A (Q161), B (Y365), D (Y346), F (all), M (all), and O (all)	None
Other	None	None	Binding assemblies 1 and 2 considered simultaneously, see section Case Study 3: Engineering <i>M. acetivorans</i> Mcr for More Rapid Product Release	None

There are several new abbreviations used within the table, namely *Methanosarcina acetivorans* (MA), ground state (GS), and product state (PS). Any parameters required to run IPRO that are not explicitly listed in the table are assumed to be their default values. These default values are prompted to the user when setting up the simulation. Molecules are listed first and are given a molecule name, followed by a description of the molecule. Target molecules are also listed beneath a header describing the molecule's state (GS, TS, or PS) The molecule's name is used when referencing it in the remainder of the table. The various input files can be found at <http://www.marangroup.com>.

radicals (Scheller et al., 2016). In this work, we revisited existing literature to compile a more complete understanding of Mcr kinetics and which steps are likely to limit the net rate of AOM. Though the temperature ranges considered in this study are industrially relevant (>20°C), the *in vivo* conditions do not mimic the *in situ* environment. The possibility remains that a separate step may limit Mcr kinetics at even lower temperatures that more closely resemble environmental conditions (~0°C) for AOM by ANME. The calculations and their underlying assumptions suggested that the rate of product, specifically CH₃-S-CoM, release limits the overall AOM kinetics. A geometric model developed by Samson and Deutch (Samson and Deutch,

1978) was used to test whether Mcr kinetics was diffusion-limited, but the derived second-order rate constant for diffusion was two orders of magnitude higher than that of methane binding (step 4 of the mechanism). Four separate case studies for improving the net AOM rate were developed, partially on the basis of these calculations.

A methanotrophic Mcr was redesigned to accept a methanogenic cofactor, assuming that the modified cofactor was exclusively important for active site rigidity. Despite the deletion of the methylthio- substituent of cofactor F₄₃₀ and its associated increase in binding cavity size, substitutions to small, hydrophobic amino acids (especially glycine) most effectively

improved binding to the methanogenic cofactor F₄₃₀. At high temperatures (>45°C), methane activation may limit the kinetics for AOM, and Mcr variants with diverse chemical properties, ranging from large and hydrophilic to small and hydrophobic, stabilize amino acids immediately adjacent to the transition state. At the low-to-mid temperature range (<45°C), large hydrophobic residues that can assume multiple conformations are favored in order to improve the rate of product release. In a final scenario, where the second step along the reverse acetoclastic pathway (i.e., Mtr) limits AOM, redesigning the substrate specificity of the more active methionine synthase homolog is achieved by introducing a positively charged residue to stabilize the negatively charged sulfonate of CH₃-S-CoM, and surprisingly few substitutions are required to accommodate the larger H₄SPT substrate. Taking these findings, later efforts can be pursued to test these variants which have the ability to not only make the conversion of methane to liquid fuels more economically viable, but also provide a deeper understanding of Mcr kinetics.

AUTHOR CONTRIBUTIONS

MG and CM conceived the case studies. MG performed the simulations and analyzed existing kinetic data from literature. JF provided guidance during the redesign procedures. CM oversaw the simulations. MG, JF, and CM wrote and edited the

manuscript. MG, JF, and CM accepted the final submitted version of the manuscript.

FUNDING

Funding was provided by the Advanced Research Projects Agency-Energy (ARPA-E, DE-AR0000431). Additional funding was provided by The Center for Bioenergy Innovation, a U.S. Department of Energy Research Center supported by the Office of Biological and Environmental Research in the DOE Office of Science (DE-AC05-00OR22725).

ACKNOWLEDGMENTS

We would like to thank the Penn State Institute for Cyberscience for maintaining the supercomputers that were used to generate designs. We would also like to thank the members of the ARPA-E REMOTE (Reducing Emissions using Methanotrophic Organisms for Transportation Energy) program for their useful conversations.

SUPPLEMENTARY MATERIAL

The Supplementary Material for this article can be found online at: <https://www.frontiersin.org/articles/10.3389/fenvs.2018.00084/full#supplementary-material>

REFERENCES

- Allen, K. D., Wegener, G., and White, R. H. (2014). Discovery of multiple modified F(430) coenzymes in methanogens and anaerobic methanotrophic archaea suggests possible new roles for F(430) in nature. *Appl. Environ. Microbiol.* 80, 6403–6412. doi: 10.1128/AEM.02202-14
- Altschul, S. F., Madden, T. L., Schaffer, A. A., Zhang, J., Zhang, Z., Miller, W., et al. (1997). Gapped BLAST and PSI-BLAST: a new generation of protein database search programs. *Nucleic Acids Res.* 25, 3389–3402. doi: 10.1093/nar/25.17.3389
- Andrews, L. D., Fenn, T. D., and Herschlag, D. (2013). Ground state destabilization by anionic nucleophiles contributes to the activity of phosphoryl transfer enzymes. *PLoS Biol.* 11:e1001599. doi: 10.1371/journal.pbio.1001599
- Arnold, K., Bordoli, L., Kopp, J., and Schwede, T. (2006). The SWISS-MODEL workspace: a web-based environment for protein structure homology modelling. *Bioinformatics* 22, 195–201. doi: 10.1093/bioinformatics/bti770
- Ashworth, J., Havranek, J. J., Duarte, C. M., Sussman, D., Monnat, R. J. Jr., Stoddard, B. L., et al. (2006). Computational redesign of endonuclease DNA binding and cleavage specificity. *Nature* 441, 656–659. doi: 10.1038/nature04818
- Beal, E. J., House, C. H., and Orphan, V. J. (2009). Manganese- and iron-dependent marine methane oxidation. *Science* 325, 184–187. doi: 10.1126/science.1169984
- Benedict, M. N., Gonnerman, M. C., Metcalf, W. W., and Price, N. D. (2012). Genome-scale metabolic reconstruction and hypothesis testing in the methanogenic archaeon *Methanosarcina acetivorans* C2A. *J. Bacteriol.* 194, 855–865. doi: 10.1128/JB.06040-11
- Bloom, J. D., Meyer, M. M., Meinhold, P., Otey, C. R., MacMillan, D., and Arnold, F. H. (2005). Evolving strategies for enzyme engineering. *Curr. Opin. Struct. Biol.* 15, 447–452. doi: 10.1016/j.sbi.2005.06.004
- Cedervall, P. E., Dey, M., Pearson, A. R., Ragsdale, S. W., and Wilmot, C. M. (2010). Structural insight into methyl-coenzyme M reductase chemistry using coenzyme B analogues. *Biochemistry* 49, 7683–7693. doi: 10.1021/bi10458d
- Chen, S.-L., Blomberg, M. R. A., and Siegbahn, P. E. M. (2012). How is methane formed and oxidized reversibly when catalyzed by nickel-containing methyl-coenzyme M reductase? *Chemistry* 18, 6309–6315. doi: 10.1002/chem.201200274
- Duan, Z. H., and Mao, S. D. (2006). A thermodynamic model for calculating methane solubility, density and gas phase composition of methane-bearing aqueous fluids from 273 to 523 K and from 1 to 2000 bar. *Geochim. Cosmochim. Acta* 70, 3369–3386. doi: 10.1016/j.gca.2006.03.018
- Ebner, S., Jaun, B., Goenrich, M., Thauer, R. K., and Harmer, J. (2010). Binding of coenzyme B induces a major conformational change in the active site of methyl-coenzyme M reductase. *J. Am. Chem. Soc.* 132, 567–575. doi: 10.1021/ja906367h
- Ellermann, J., Hedderich, R., Bocher, R., and Thauer, R. K. (1988). The final step in methane formation. Investigations with highly purified methyl-CoM reductase (component C) from *Methanobacterium thermoautotrophicum* (strain Marburg). *Eur. J. Biochem.* 172, 669–677. doi: 10.1111/j.1432-1033.1988.tb13941.x
- Ermiler, U., Grabarse, W., Shima, S., Goubeaud, M., and Thauer, R. K. (1997). Crystal structure of methyl coenzyme M reductase: the key enzyme of biological methane formation. *Science* 278, 1457–1462.
- Evans, J. C., Huddler, D. P., Hilgers, M. T., Romanchuk, G., Matthews, R. G., and Ludwig, M. L. (2004). Structures of the N-terminal modules imply large domain motions during catalysis by methionine synthase. *Proc. Natl. Acad. Sci. U.S.A.* 101, 3729–3736. doi: 10.1073/pnas.0308082100
- Faiella, M., Andreozzi, C., de Rosales, R. T., Pavone, V., Maglio, O., Nastro, F., et al. (2009). An artificial di-iron oxo-protein with phenol oxidase activity. *Nat. Chem. Biol.* 5, 882–884. doi: 10.1038/nchembio.257
- Fazelina, H., Cirino, P. C., and Maranas, C. D. (2007). Extending iterative protein redesign and optimization (IPRO) in protein library design for ligand specificity. *Biophys. J.* 92, 2120–2130. doi: 10.1529/biophysj.106.096016
- Garrabou, X., Wicky, B. I., and Hilvert, D. (2016). Fast Knoevenagel condensations catalyzed by an artificial schiff-base-forming enzyme. *J. Am. Chem. Soc.* 138, 6972–6974. doi: 10.1021/jacs.6b00816

- Goubeaud, M., Schreiner, G., and Thauer, R. K. (1997). Purified methyl-coenzyme M reductase is activated when the enzyme-bound coenzyme F430 is reduced to the Nickel(I) oxidation state by titanium(III) citrate. *Eur. J. Biochem.* 243, 110–114. doi: 10.1111/j.1432-1033.1997.00110.x
- Grabarse, W., Mahlert, F., Duin, E. C., Goubeaud, M., Shima, S., Thauer, R. K., et al. (2001). On the mechanism of biological methane formation: structural evidence for conformational changes in methyl-coenzyme M reductase upon substrate binding. *J. Mol. Biol.* 309, 315–330. doi: 10.1006/jmbi.2001.4647
- Grabarse, W., Mahlert, F., Shima, S., Thauer, R. K., and Ermler, U. (2000). Comparison of three methyl-coenzyme M reductases from phylogenetically distant organisms: unusual amino acid modification, conservation and adaptation. *J. Mol. Biol.* 303, 329–344. doi: 10.1006/jmbi.2000.4136
- Grisewood, M. J., Gifford, N. P., Pantazes, R. J., Li, Y., Cirino, P. C., Janik, M. J., et al. (2013). OptZyme: computational enzyme redesign using transition state analogues. *PLoS ONE* 8:e75358. doi: 10.1371/journal.pone.0075358
- Grisewood, M. J., Hernández-Lozada, N. J., Thoden, J. B., Gifford, N. P., Mendez-Perez, D., Schoenberger, H. A., et al. (2017). Computational redesign of acyl-ACP thioesterase with improved selectivity toward medium-chain-length fatty acids. *ACS Catal.* 7, 3837–3849. doi: 10.1021/acscatal.7b00408
- Hallam, S. J., Putnam, N., Preston, C. M., Detter, J. C., Rokhsar, D., Richardson, P. M., et al. (2004). Reverse methanogenesis: testing the hypothesis with environmental genomics. *Science* 305, 1457–1462. doi: 10.1126/science.1100025
- Harmer, J., Finazzo, C., Piskorski, R., Ebner, S., Duin, E. C., Goenrich, M., et al. (2008). A nickel hydride complex in the active site of methyl-coenzyme M reductase: implications for the catalytic cycle. *J. Am. Chem. Soc.* 130, 10907–10920. doi: 10.1021/ja710949e
- Haroön, M. F., Hu, S., Shi, Y., Imelfort, M., Keller, J., Hugenholtz, P., et al. (2013). Anaerobic oxidation of methane coupled to nitrate reduction in a novel archaeal lineage. *Nature* 500, 567–570. doi: 10.1038/nature12375
- Haynes, C. A., and Gonzalez, R. (2014). Rethinking biological activation of methane and conversion to liquid fuels. *Nat. Chem. Biol.* 10, 331–339. doi: 10.1038/nchembio.1509
- Heller, C., Hoppert, M., and Reitner, J. (2008). Immunological localization of coenzyme M reductase in anaerobic methane-oxidizing archaea of ANME 1 and ANME 2 type. *Geomicrobiol. J.* 25, 149–156. doi: 10.1080/01490450802006884
- Hilvert, D. (2013). Design of protein catalysts. *Annu. Rev. Biochem.* 82, 447–470. doi: 10.1146/annurev-biochem-072611-101825
- Hinrichs, K.-U., and Boetius, A. (2003). “The anaerobic oxidation of methane: new insights in microbial ecology and biogeochemistry,” in *Ocean Margin Systems*, eds G. Wefer, D. Billett, D. Hebbeln, B. B. Jørgensen, M. Schlüter, and T. C. E. van Weering (Heidelberg: Springer Berlin Heidelberg), 457–477.
- Hoehler, T. M., Alperin, M. J., Albert, D. B., and Martens, C. S. (1994). Field and laboratory studies of methane oxidation in an anoxic marine sediment - evidence for a methanogen-sulfate reducer consortium. *Glob. Biogeochem. Cycles* 8, 451–463. doi: 10.1029/94GB01800
- Huang, P. S., Boyken, S. E., and Baker, D. (2016). The coming of age of *de novo* protein design. *Nature* 537, 320–327. doi: 10.1038/nature19946
- Huang, S., Romanchuk, G., Patridge, K., Lesley, S. A., Wilson, I. A., Matthews, R. G., et al. (2007). Reactivation of methionine synthase from thermotoga maritima (TM0268) requires the downstream gene product TM0269. *Protein Sci.* 16, 1588–1595. doi: 10.1110/ps.072936307
- Jiang, L., Althoff, E. A., Clemente, F. R., Doyle, L., Rothlisberger, D., Zanghellini, A., et al. (2008). *De novo* computational design of retro-aldol enzymes. *Science* 319, 1387–1391. doi: 10.1126/science.1152692
- Kahnt, J., Buchenau, B., Mahlert, F., Kruger, M., Shima, S., and Thauer, R. K. (2007). Post-translational modifications in the active site region of methyl-coenzyme M reductase from methanogenic and methanotrophic archaea. *FEBS J.* 274, 4913–4921. doi: 10.1111/j.1742-4658.2007.06016.x
- Kamerlin, S. C. L., Florian, J., and Warshel, A. (2008). Associative versus dissociative mechanisms of phosphate monoester hydrolysis: on the interpretation of activation entropies. *Chem. Phys. Chem.* 9, 1767–1773. doi: 10.1002/cphc.200800356
- Knittel, K., and Boetius, A. (2009). Anaerobic oxidation of methane: progress with an unknown process. *Annu. Rev. Microbiol.* 63, 311–334. doi: 10.1146/annurev.micro.61.080706.093130
- Krüger, M., Meyerdierks, A., Glockner, F. O., Amann, R., Widdel, F., Kube, M., et al. (2003). A conspicuous nickel protein in microbial mats that oxidize methane anaerobically. *Nature* 426, 878–881. doi: 10.1038/nature02207
- Lazaridis, T., and Karplus, M. (1999). Effective energy function for proteins in solution. *Proteins* 35, 133–152. doi: 10.1002/(SICI)1097-0134(19990501)35:2<133::AID-PROT1>3.0.CO;2-N
- Lee, M. S., Feig, M., Salsbury, F. R., and Brooks, C. L. (2003). New analytic approximation to the standard molecular volume definition and its application to generalized born calculations. *J. Comput. Chem.* 24, 1821–1821. doi: 10.1002/jcc.10367
- Lu, Y.-Z., Fu, L., Ding, J., Ding, Z.-W., Li, N., and Zeng, R. J. (2016). Cr(VI) reduction coupled with anaerobic oxidation of methane in a laboratory reactor. *Water Res.* 102, 445–452. doi: 10.1016/j.watres.2016.06.065
- Marchler-Bauer, A., Derbyshire, M. K., Gonzales, N. R., Lu, S. N., Chitsaz, F., Geer, L. Y., et al. (2015). Cdd: NCBI’s conserved domain database. *Nucleic Acids Res.* 43, D222–D226. doi: 10.1093/nar/gku1221
- Mayr, S., Latkoczy, C., Kruger, M., Gunther, D., Shima, S., Thauer, R. K., et al. (2008). Structure of an F430 variant from archaea associated with anaerobic oxidation of methane. *J. Am. Chem. Soc.* 130, 10758–10767. doi: 10.1021/ja802929z
- McGlynn, S. E., Chadwick, G. L., Kempes, C. P., and Orphan, V. J. (2015). Single cell activity reveals direct electron transfer in methanotrophic consortia. *Nature* 526, 531–535. doi: 10.1038/nature15512
- Meyer, M. M., Hochrein, L., and Arnold, F. H. (2006). Structure-guided SCHEMA recombination of distantly related beta-lactamases. *Protein Eng. Des. Selection* 19, 563–570. doi: 10.1093/protein/gz1045
- Moore, G. L., and Maranas, C. D. (2004). Computational challenges in combinatorial library design for protein engineering. *AIChE J.* 50, 262–272. doi: 10.1002/aic.10025
- Moran, J. J., House, C. H., Freeman, K. H., and Ferry, J. G. (2005). Trace methane oxidation studied in several *Euryarchaeota* under diverse conditions. *Archaea* 1, 303–309. doi: 10.1155/2005/650670
- Moran, J. J., House, C. H., Thomas, B., and Freeman, K. H. (2007). Products of trace methane oxidation during nonmethylotrophic growth by *Methanosarcina*. *J. Geophys. Res. Biogeosci.* 112, 1–7. doi: 10.1029/2006JG000268
- Mueller, T. J., Grisewood, M. J., Nazem-Bokae, H., Gopalakrishnan, S., Ferry, J. G., Wood, T. K., et al. (2015). Methane oxidation by anaerobic archaea for conversion to liquid fuels. *J. Ind. Microbiol. Biotechnol.* 42, 391–401. doi: 10.1007/s10295-014-1548-7
- Murphy, P. M., Bolduc, J. M., Gallaher, J. L., Stoddard, B. L., and Baker, D. (2009). Alteration of enzyme specificity by computational loop remodeling and design. *Proc. Natl. Acad. Sci. U.S.A.* 106, 9215–9220. doi: 10.1073/pnas.0811070106
- Nauhaus, K., Treude, T., Boetius, A., and Kruger, M. (2005). Environmental regulation of the anaerobic oxidation of methane: a comparison of ANME-I and ANME-II communities. *Environ. Microbiol.* 7, 98–106. doi: 10.1111/j.1462-2920.2004.00669.x
- Nazem-Bokae, H., Gopalakrishnan, S., Ferry, J. G., Wood, T. K., and Maranas, C. D. (2016). Assessing methanotrophy and carbon fixation for biofuel production by *Methanosarcina acetivorans*. *Microb. Cell Fact.* 15:10. doi: 10.1186/s12934-015-0404-4
- Packer, M. S., and Liu, D. R. (2015). Methods for the directed evolution of proteins. *Nat. Rev. Genet.* 16, 379–394. doi: 10.1038/nrg3927
- Pantazes, R. J., Grisewood, M. J., Li, T., Gifford, N. P., and Maranas, C. D. (2015). The iterative protein redesign and optimization (IPRO) suite of programs. *J. Comput. Chem.* 36, 251–263. doi: 10.1002/jcc.23796
- Pantazes, R. J., Grisewood, M. J., and Maranas, C. D. (2011). Recent advances in computational protein design. *Curr. Opin. Struct. Biol.* 21, 467–472. doi: 10.1016/j.sbi.2011.04.005
- Pantazes, R. J., Saraf, M. C., and Maranas, C. D. (2007). Optimal protein library design using recombination or point mutations based on sequence-based scoring functions. *Protein Eng. Des. Sel.* 20, 361–373. doi: 10.1093/protein/gzm030
- Phillips, R. S., Vita, A., Spivey, J. B., Rudloff, A. P., Driscoll, M. D., and Hay, S. (2016). Ground-State destabilization by Phe-448 and Phe-449 contributes to tyrosine phenol-lyase catalysis. *ACS Catal.* 6, 6770–6779. doi: 10.1021/acscatal.6b01495

- Pommié, C., Levadoux, S., Sabatier, R., Lefranc, G., and Lefranc, M. P. (2004). IMGT standardized criteria for statistical analysis of immunoglobulin V-REGION amino acid properties. *J. Molecul. Recognit.* 17, 17–32. doi: 10.1002/jmr.647
- Ragsdale, S. W., Raugei, S., Ginovska, B., and Wongnate, T. (2017). “Biochemistry of methyl-coenzyme M reductase,” in *The Biological Chemistry of Nickel*, eds D. Zamble, M. Rowinska-Zyrek, and H. Kozlowski (Cambridge: The Royal Society of Chemistry), 149–169.
- Reeburgh, W. S. (1996). “Soft Spots’ in the Global Methane Budget,” in *Microbial Growth on C₁ Compounds*, eds M. E. Lidstrom and F. R. Tabita (Dordrecht: Kluwer Academic), 334–342.
- Reeve, J. N., Nolling, J., Morgan, R. M., and Smith, D. R. (1997). Methanogenesis: genes, genomes, and who’s on first? *J. Bacteriol.* 179, 5975–5986. doi: 10.1128/jb.179.19.5975-5986.1997
- Richter, F., Blomberg, R., Khare, S. D., Kiss, G., Kuzin, A. P., Smith, A. J., et al. (2012). Computational design of catalytic dyads and oxyanion holes for ester hydrolysis. *J. Am. Chem. Soc.* 134, 16197–16206. doi: 10.1021/ja3037367
- Röthlisberger, D., Khersonsky, O., Wollacott, A. M., Jiang, L., DeChancie, J., Betker, J., et al. (2008). Kemp elimination catalysts by computational enzyme design. *Nature* 453, U190–U194. doi: 10.1038/nature06879
- Ruben, E. A., Schwans, J. P., Sonnett, M., Natarajan, A., Gonzalez, A., Tsai, Y., et al. (2013). Ground state destabilization from a positioned general base in the ketosteroid isomerase active site. *Biochemistry* 52, 1074–1081. doi: 10.1021/bi301348x
- Rüdiger, H., and Jaenicke, L. (1969). Methionine synthesis: demonstration of the reversibility of the reaction. *FEBS Lett.* 4, 316–318. doi: 10.1016/0014-5793(69)80264-4
- Samson, R., and Deutch, J. M. (1978). Diffusion-controlled reaction rate to a buried active site. *J. Chem. Phys.* 68, 285–290. doi: 10.1063/1.435494
- Saraf, M. C., Moore, G. L., Goodey, N. M., Cao, V. Y., Benkovic, S. J., and Maranas, C. D. (2006). IPRO: an iterative computational protein library redesign and optimization procedure. *Biophys. J.* 90, 4167–4180. doi: 10.1529/biophysj.105.079277
- Scheller, S., Goenrich, M., Boecher, R., Thauer, R. K., and Jaun, B. (2010). The key nickel enzyme of methanogenesis catalyses the anaerobic oxidation of methane. *Nature* 465, 606–608. doi: 10.1038/nature09015
- Scheller, S., Goenrich, M., Thauer, R. K., and Jaun, B. (2013). Methyl-coenzyme M reductase from methanogenic archaea: isotope effects on the formation and anaerobic oxidation of methane. *J. Am. Chem. Soc.* 135, 14975–14984. doi: 10.1021/ja406485z
- Scheller, S., Yu, H., Chadwick, G. L., McGlynn, S. E., and Orphan, V. J. (2016). Artificial electron acceptors decouple archaeal methane oxidation from sulfate reduction. *Science* 351, 703–707. doi: 10.1126/science.aad7154
- Shima, S., Krueger, M., Weinert, T., Demmer, U., Kahnt, J., Thauer, R. K., et al. (2012). Structure of a methyl-coenzyme M reductase from black sea mats that oxidize methane anaerobically. *Nature* 481, 98–101. doi: 10.1038/nature10663
- Siegel, J. B., Zanghellini, A., Lovick, H. M., Kiss, G., Lambert, A. R., St Clair, J. L., et al. (2010). Computational design of an enzyme catalyst for a stereoselective bimolecular Diels-Alder reaction. *Science* 329, 309–313. doi: 10.1126/science.1190239
- Sievers, F., Wilm, A., Dineen, D., Gibson, T. J., Karplus, K., Li, W., et al. (2011). Fast, scalable generation of high-quality protein multiple sequence alignments using Clustal Omega. *Mol. Syst. Biol.* 7: 539. doi: 10.1038/msb.2011.75
- Soo, V. W., McAnulty, M. J., Tripathi, A., Zhu, F., Zhang, L., Hatzakis, E., et al. (2016). Reversing methanogenesis to capture methane for liquid biofuel precursors. *Microb. Cell Fact.* 15, 11. doi: 10.1186/s12934-015-0397-z
- Thauer, R. K. (2011). Anaerobic oxidation of methane with sulfate: on the reversibility of the reactions that are catalyzed by enzymes also involved in methanogenesis from CO₂. *Curr. Opin. Microbiol.* 14, 292–299. doi: 10.1016/j.mib.2011.03.003
- Thauer, R. K., and Shima, S. (2008). Methane as fuel for anaerobic microorganisms. *Ann. N. Y. Acad. Sci.* 1125, 158–170. doi: 10.1196/annals.1419.000
- UniProt, C. (2015). UniProt: a hub for protein information. *Nucleic Acids Res.* 43, D204–D212. doi: 10.1093/nar/gku989
- Vanommeslaeghe, K., and MacKerell, A. D. Jr. (2012). Automation of the CHARMM General Force Field (CGenFF) I: bond perception and atom typing. *J. Chem. Inf. Model.* 52, 3144–3154. doi: 10.1021/ci300363c
- Vanommeslaeghe, K., Raman, E. P., and MacKerell, A. D. Jr. (2012). Automation of the CHARMM general force field (CGenFF) II: assignment of bonded parameters and partial atomic charges. *J. Chem. Inf. Model.* 52, 3155–3168. doi: 10.1021/ci3003649
- Vepachedu, V. R., and Ferry, J. G. (2012). Role of the fused corrinoid/methyl transfer protein CmtA during CO-dependent growth of *Methanosarcina acetivorans*. *J. Bacteriol.* 194, 4161–4168. doi: 10.1128/JB.00593-12
- Wegener, G., Krukenberg, V., Riedel, D., Tegetmeyer, H. E., and Boetius, A. (2015). Intercellular wiring enables electron transfer between methanotrophic archaea and bacteria. *Nature* 526, 587–590. doi: 10.1038/nature15733
- Wongnate, T., and Ragsdale, S. W. (2015). The reaction mechanism of methyl-coenzyme M reductase: how an enzyme enforces strict binding order. *J. Biol. Chem.* 290, 9322–9334. doi: 10.1074/jbc.M115.636761
- Wongnate, T., Sliwa, D., Ginovska, B., Smith, D., Wolf, M. W., Lehnert, N., et al. (2016). The radical mechanism of biological methane synthesis by methyl-coenzyme M reductase. *Science* 352, 953–958. doi: 10.1126/science.aaf0616
- Xiao, H., Bao, Z. H., and Zhao, H. M. (2015). High throughput screening and selection methods for directed enzyme evolution. *Ind. Eng. Chem. Res.* 54, 4011–4020. doi: 10.1021/ie503060a
- Yan, Z., Joshi, P., Gorski, C. A., and Ferry, J. G. (2018). A biochemical framework for anaerobic oxidation of methane driven by Fe(III)-dependent respiration. *Nat. Commun.* 9:1642. doi: 10.1038/s41467-018-04097-9
- Zheng, K., Ngo, P. D., Owens, V. L., Yang, X. P., and Mansoorabadi, S. O. (2016). The biosynthetic pathway of coenzyme F₄₃₀ in methanogenic and methanotrophic archaea. *Science* 354, 339–342. doi: 10.1126/science.aag2947
- Zhou, Y., Dorchak, A. E., and Ragsdale, S. W. (2013). *In vivo* activation of methyl-coenzyme M reductase by carbon monoxide. *Front. Microbiol.* 4:69. doi: 10.3389/fmicb.2013.00069

Conflict of Interest Statement: The authors declare that the research was conducted in the absence of any commercial or financial relationships that could be construed as a potential conflict of interest.

Copyright © 2018 Grisewood, Ferry and Maranas. This is an open-access article distributed under the terms of the Creative Commons Attribution License (CC BY). The use, distribution or reproduction in other forums is permitted, provided the original author(s) and the copyright owner(s) are credited and that the original publication in this journal is cited, in accordance with accepted academic practice. No use, distribution or reproduction is permitted which does not comply with these terms.